California Institute of Technology

Power Electronics Group

EE 116–81

Pasadena, CA 91125

(818) 356-4781

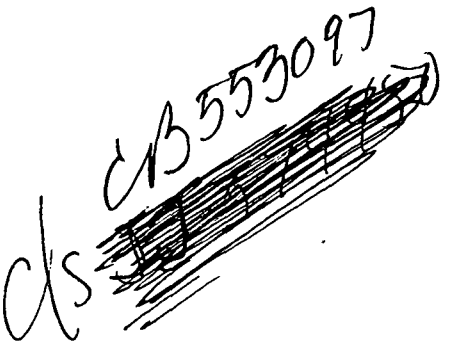

Final Report

Input-Current Shaped Ac-to-Dc Converters

Prepared for

NASA Lewis Research Center

under

Grant No. NAG 3-615

May 1986

Abstract

The problem of achieving near-unity power factor while supplying power to a dc load from a single-phase ac source of power is examined. Power processors for this application must perform three functions: input-current shaping, energy storage, and output-voltage regulation. The methods available for performing each of these three functions are reviewed. Input-current shaping methods are either active or passive, with the active methods divided into buck-like and boost-like techniques. In addition to large reactances, energy storage methods include resonant filters, active filters, and active storage schemes. Fast voltage regulation can be achieved by post-regulation or by supplementing the current-shaping topology with an extra switch. Some indication of which methods are best suited for particular applications concludes the discussion.

Contents

ELECTRIC POWER SUPPLIES
CURRENT CONVERTERS (AC TO DC)
VOLTAGE REGULATORS
ELECTRIC ENERGY STORAGE

ELECTRIC SWITCHES
SWITCHING CIRCUITS
REACTANCE
INDUCTANCE

1 Introduction

In switched-mode power conversion, a high quality output voltage is usually of first importance. Converters are often chosen for their ability to produce clean, well-regulated outputs while problems with the input side are ignored or patched up with filters.

The present proliferation of switching converters and other non-linear loads is changing this approach, forcing designers to consider converters as generators of input current, as well as of output voltage, waveforms.

The objective of this work is to investigate and catalog input-current shaping techniques for power converters supplying dc loads from a single-phase ac line. Three-phase power sources present a quite different set of problems and are outside the scope of this report. The demand for input-current improvement is first reviewed, along with some means of describing the quality of input waveforms. A current-shaping converter is found to perform at least three vital functions, detailed in Section 1.3, and two fundamental restrictions on the operation of *all* current shapers are discussed in Section 2. Section 3 examines techniques for generating input-current waveforms, and Section 4 presents ways of handling the energy storage problem identified in Section 2.1. A novel method of combining current shaping and fast voltage regulation in the same topology is presented in Section 5. The merits of each technique are summarized in Section 6, and conclusions are drawn regarding the best techniques for certain applications.

1.1 Need for Current Shaping

There are two major reasons why increased attention needs to be given to input-current shaping for ac-to-dc power converters, both of which lead to the conclusion that the input-current waveshape should be the same as that of the input voltage, and in phase with it. In other words, the input current and voltage at every instant should be related by a real constant, just as if the load were a resistor instead of a power converter. For a sinusoidal input voltage, the case considered here, the input current should therefore be a sine wave in phase with the input voltage.

Efficiency

The first reason concerns high efficiency. Any periodic current or voltage waveform may be represented by a Fourier series. Only Fourier components of the current that match those of the voltage waveform deliver power from source to load; however, all current components contribute to the rms value of the current, and hence to the lost power. Therefore, any current component of a frequency not present in the voltage waveform, or of the wrong phase, generates power loss in the parasitic resistance but does not contribute to the load power. For a given rms current (given parasitic loss), maximum power is delivered from source to load when all current Fourier components are proportional to and in phase with a corresponding voltage component. Equivalently, for maximum power delivery every current component must be related to its corresponding voltage component by a common scalar, and so the entire current waveform is just a scalar multiple of the voltage waveform.

Parasitic resistance will always be present—in the converter input circuitry, in the line connecting the power source to the converter, and in the source itself (source resistance). Parasitic power loss in excess of the minimum leads not only to loss of electrical efficiency, but also to poor utilization of source and line capacity.

Noise

The second reason why the input current should be the same as the voltage waveform is that otherwise unnecessary noise is generated, both radiated and conducted. In a converter operating from a dc input voltage, any ac component of input current can be considered as noise. There are two sources of such noise: reflected load current, and internally generated ac currents caused by the switching action of the converter, which consist of the switching frequency and its harmonics.

In a converter operating from an ac input voltage, noise currents are those of frequencies other than the line frequency. This noise comes not only from the load and from the internal switching action, but also from harmonics of the line frequency caused by rectification of the input voltage. These harmonics can be large, as in the common half-wave, full-wave, or bridge rectifiers followed by a large reservoir capacitor. Sidebands generated by the switching frequency in combination with the line frequency may also be present.

1.2 Power Factor

One measure of how close a current waveform comes to the ideal is the *power factor*, or PF. In general, power factor is defined as the ratio of true power to the product of rms voltage and rms current. When the line voltage is a distortion-free sinusoid, however, a more useful special case of this definition is

$$\mathrm{PF} = \frac{I_f}{I_t} \cos\phi \tag{1}$$

where ϕ is the angle the fundamental component of the current makes with the voltage, I_f is the rms value of the fundamental of the current, and I_t is the rms value of the total current. Equation (1) shows that power factor degradation comes from two sources—phase displacement of the fundamental component of the current, and current waveform distortion. In the case of a linear load, the current is sinusoidal and only phase displacement, $\cos\phi$, reduces the PF below unity. Rectifiers and switching converters present a nonlinear load to the line, and the distortion factor, I_f/I_t contributes to PF reduction. Pure sinusoidal, in-phase current is the *only* way to obtain unity PF, but if lower PF's are acceptable then the loss may be taken as phase displacement or distortion, or as a combination of both.

1.3 Functions of an Input-Current Shaper

The difficulties of input-current shaping depend heavily on the power source (line) and load to be matched. The only case considered here is the common problem of supplying a dc load from a single-phase line. Allowing a three-phase power source

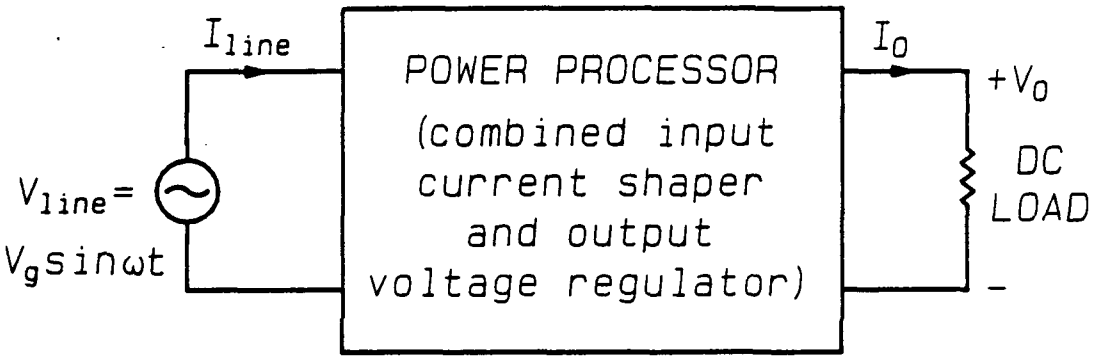

Figure 1: Power processor supplying a dc load from a single-phase ac power source.

removes the energy storage restriction discussed in Section 2.1, permitting alternatives not available with a single-phase source.

Figure 1 shows the system of interest. The power processor, or "input-current shaper," draws power from the single-phase power source and supplies constant power to the load. The load, in steady-state, is modeled as a resistor of value $R_L = V_o/I_o$.

An ideal power processor for the application of Fig.1 would have unity PF and high bandwidth control over the output voltage. It would also have high efficiency and low weight, complexity, and cost. The many current-shaping methods available each trade strength in some of these areas for weakness in others.

The input-current shaper of Fig.1 must perform three functions. One function is, of course, shaping the input-current waveform. A sinusoidal current is most desirable, but a current shaper may be called upon to impose other waveforms. Section 3 presents several shaping methods. Because the current shaper supplies constant power to the load while the input current is *not* constant, the shaper must take up and give back energy during each line cycle. Thus a second function of a current shaper is to "balance" the difference between input and output power. This power balancing requires the power processor to store at least a *minimum* amount of energy, independent of the internal switching frequency, as discussed in Section 2.1. Section 4 compares various methods of handling the energy storage problem. Finally, output voltage regulation must be included in the power processor of Fig.1. Regulation may be performed by the same circuitry that shapes the input current or by a separate dc-to-dc converter. Section 2.2 discusses the challenges of simultaneous input current and output voltage control, and Section 5 shows how an added switch can enable a current-shaping converter to rapidly regulate the output voltage.

2 Fundamental Limitations of Current Shapers

It is often the case in power processing that, theoretically, if one could only

switch fast enough, problems of weight and speed of response would disappear. Input-current shapers do not follow this "rule." Instead, they have fundamental restrictions on stored energy and speed of response that are independent of switching frequency. First, absorbing the difference between the varying input power and the constant load power requires a minimum amount of energy storage in the power processor. Second, control variables that are used to shape input current cannot also be used to provide high bandwidth control of the output voltage. An extra degree of freedom—in this case a switch—is necessary to achieve both input-current shaping and fast control over the output voltage.

2.1 Minimum Stored Energy

The amount of energy a current-shaping power processor must store to balance the difference between input and output power will depend upon the input-current waveform. The stored energy requirement is found here for the ideal case of sinusoidal, in-phase current. Other, less ideal, waveforms may yield slightly different theoretical requirements, but the important result remains that a current shaper must store energy, and the minimum amount stored is limited by the line frequency and the load power level, regardless of internal switching frequency.

Consider a converter with 100 percent efficiency drawing an in-phase, sinusoidal current from the line and delivering constant power P to a load, as in Fig.2. Because the input voltage and current both vary as $\sin \omega t$, the input power is $2P \sin^2 \omega t$ or $P - P \cos 2\omega t$. The difference between the input power and the output power is absorbed by the converter. Since no energy can be lost, this power difference must alternately increase and decrease the stored energy of the converter. The change in stored energy is the integral of the absorbed power, plus some constant.

$$U(t) = \int -P \cos 2\omega t \, dt = -\frac{P \sin 2\omega t}{2\omega} + U(0) \tag{2}$$

The stored energy must always be positive so the minimum value of $U(0)$ must be $P/2\omega$. The peak stored energy is then

$$U_{peak} \geq \frac{P}{\omega} \tag{3}$$

The converter must contain a set of inductors and/or capacitors that store at least this amount of energy at some point in each half cycle of the line voltage.

This restriction on stored energy does *not* apply to converters running from a three-phase line, because power drawn from the three-phase line by sinusoidal currents is constant. With constant load power, no imbalance of input and output power need be absorbed by the power converter. Minimum stored energy can be a function of the switching, not the line frequency, and the reactive elements can therefore be smaller.

In addition to reduced size, weight, and cost, low stored energy is desirable for one more important reason. If the energy storage element directly feeds the load, then the ability to control the load voltage depends on changing the voltage or current through the energy storage device. Excessive stored energy means a slow time constant between the energy storage and the load, and therefore slow response to load variations or voltage change commands.

Section 4 discusses several different ways to handle the energy storage problem.

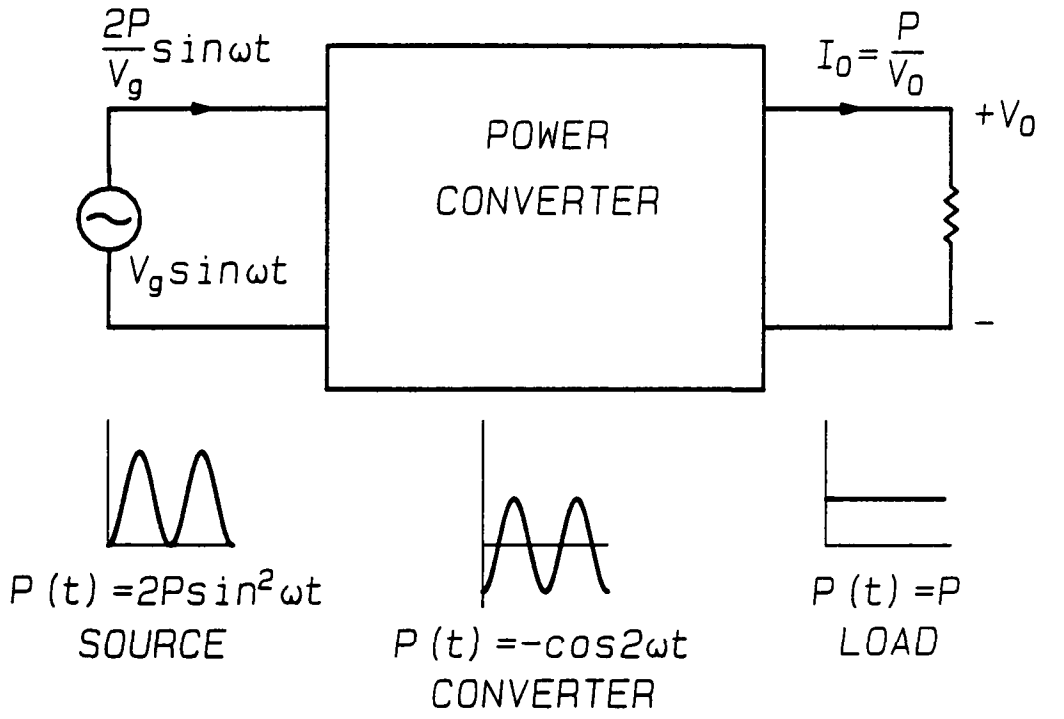

Figure 2: Ac-to-dc power converter and corresponding power waveforms.

2.2 Voltage Regulation

The control circuits of an active input-current shaper must perform two tasks. First, the controller imposes the *shape* of the input current, usually a sine wave. Second, the *amplitude* of the input waveform is adjusted so that the average power drawn from the line just equals the load power plus any losses in the converter. The second task usually corresponds to controlling the load voltage.

When the power processor has only one switch—one control variable—the following problem arises. If the bandwidth of the amplitude control loop is on the order of (or higher than) the line frequency, disturbances in this loop (output voltage ripple, for instance) will affect the shape of the input current as the current amplitude is rapidly altered within the space of a half period of the line. The amplitude loop will override the shaping control, making the latter ineffective. To avoid this problem, the bandwidth of the voltage control loop is restricted to much less than the line frequency. A converter with only one switch must therefore be an extremely slow voltage controller. Fast control of the output voltage is sacrificed to enable fast control, i.e., shaping, of the input current.

Fast voltage regulation can be recovered by adding another degree of control. Placing a complete dc-to-dc converter between the current shaper and the load is one way to get fast control over the output voltage, and this method also allows easy introduction of isolation. Section 5 gives another alternative, the three switched-network

topologies, in which adding a single switch and rectifier to the shaping topology enables fast, independent voltage regulation. Isolation is a simple matter with these topologies.

3 Input-Current Shaping Methods

An input-current waveform can be imposed by either active or passive methods. Passive methods have the advantage of simplicity, but the current waveform is generally load dependent. Active schemes offer possibilities for advanced control, such as current limiting and load-independent waveshapes. Section 3.1 discusses three passive means of current shaping and Section 3.2 introduces some of the many active schemes available.

3.1 Passive Shaping Methods

Input current can be shaped using no switches at all. In this case the power processor is really just a filter, and a dc-to-dc post-converter is required to regulate the load voltage. Passive current shapers generally need more stored energy and hence larger reactances than active methods, but they deserve consideration for their ruggedness and simplicity.

In the rare event of a high frequency power source, passive filters will be more attractive, and active methods less so, than at the usual 60 or 400Hz line frequency. For fixed performance, the value of reactances in passive filters is inversely proportional to the line frequency. Active current-shaping schemes, for constant performance, must have switching frequencies a fixed ratio above the line frequency. As line frequency increases, then, passive filters get smaller and active methods must switch faster. At some point, passive methods will be superior, and this point is by no means necessarily in the kilohertz range. Passive filters are quite common at 60Hz, although they usually do not provide power factors above 0.7 or 0.8.

The inductor input filter is probably the most common passive filter used. The filter is simple and relatively cheap. Its main drawbacks are a 0.90 upper limit on PF, and discontinuous input current for high PF. A series resonant filter is an alternative way to passively shape input current. Although heavy and expensive, it shows that unity PF is possible without using active elements. More often used as a voltage regulator, the ferroresonant transformer can also be considered as a passive current shaper. It too has a resonant circuit that makes the input current nearly sinusoidal.

3.1.1 Inductor Input Filter

A simple way to improve the input-current performance of a capacitor input filter is to place an inductor in series with the output of the bridge rectifier (Fig.3). This configuration is called the inductor input filter, by analogy with the capacitor input filter. In analyzing the filter, the usual assumption is that the output voltage is pure dc. Several analyses appear in the literature [1],[2]. A summary of the analysis and results is presented here with an emphasis on exposing the effects of inductance L, line (radian) frequency ω or line period T, and load R simultaneously. The conduction parameter K_l,

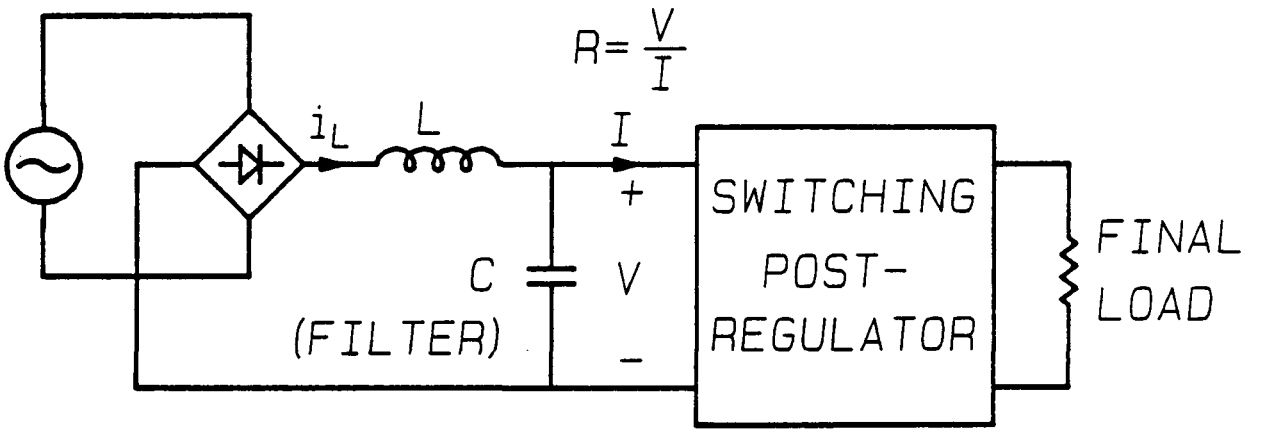

Figure 3: Inductor input filter followed by a voltage post-regulator.

defined by

$$K_l \equiv \frac{\omega L}{\pi R} = \frac{2L}{RT} \tag{4}$$

does this very well and supplants the normalized units of [1] and [2]. Note that the load R is defined as the ratio of average voltage and current at the output of the filter, and does not necessarily represent an actual resistance. The "*l*" subscript on K_l means that K_l involves the *line* frequency.

The filter operates in either the continuous conduction mode (CCM), in which the rectifier bridge always conducts, or in the discontinuous mode (DCM) when the bridge is off during some portion of the line period.

Figure 4 is an equivalent circuit for CCM. The capacitor is assumed infinitely large so that the output voltage is constant. Since the average voltage across the inductor must be zero, the output voltage is

$$V = \frac{2}{\pi} V_g \tag{5}$$

where V_g is the *peak* value of the line voltage. Integration of the voltage across the inductor gives the shape of the inductor current. The average current, or constant of integration, is chosen to produce V across R, yielding

$$i_L(\omega t) = \frac{V_g}{\omega L}\left[1 + 2K_l - \cos(\omega t) - \frac{2\omega t}{\pi}\right] \ , \ 0 < \omega t < \pi \tag{6}$$

The rms value of the line current is the same as the rms value of i_L,

$$i_{L\text{rms}} = \frac{2V_g}{\pi R}\sqrt{1 + (\frac{5}{24} - \frac{2}{\pi^2})/K_l^2} \tag{7}$$

found by integrating the square of Eq.(6). The power factor follows directly from Eqs.(5) through (7), and is a function *only* of K_l.

$$\text{PF} = \frac{2\sqrt{2}}{\pi} \frac{1}{\sqrt{1 + (\frac{5}{24} - \frac{2}{\pi^2})/K_l^2}} \approx \frac{0.90}{\sqrt{1 + (\frac{0.075}{K_l})^2}} \tag{8}$$

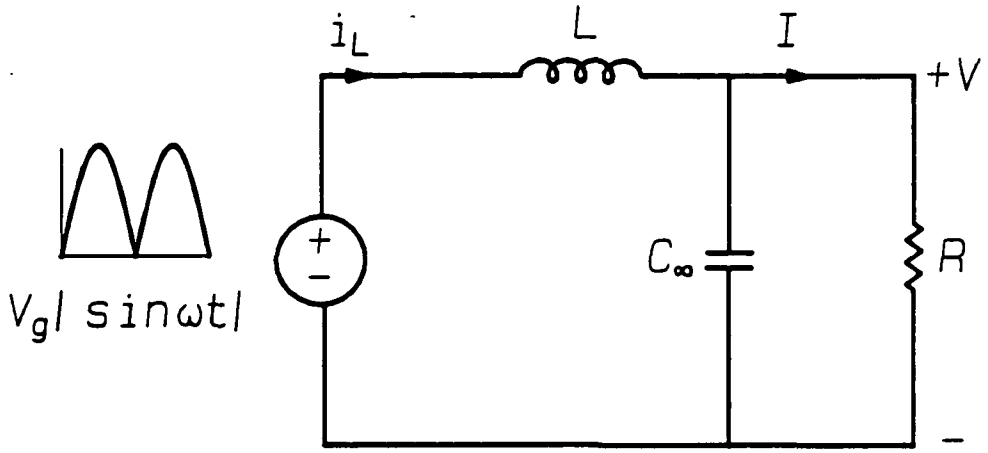

Figure 4: Equivalent circuit of the inductor input filter in CCM.

The phase displacement contribution to power factor degradation, $\cos\phi$, is found by calculating the Fourier sine and cosine coefficients of the input current, the odd extension of Eq.(6) into the full line period, and is given by

$$\cos\phi = \frac{1}{\sqrt{1+(\frac{\pi}{8}-\frac{1}{\pi})^2/K_l^2}} \approx \frac{1}{\sqrt{1+(\frac{0.074}{K_l})^2}} \tag{9}$$

The boundary of CCM, called critical conduction, occurs when the current of Eq.(6) just reaches zero at some point during a cycle. Equation (6) can be differentiated to find that the minimum current occurs when

$$\omega t = \sin^{-1}\left(\frac{2}{\pi}\right) \approx 40° \tag{10}$$

The value of K_l that makes the current exactly zero at this point is found to be

$$K_{l\,\text{crit}} = \frac{1}{2}\left\{\frac{2}{\pi}\sin^{-1}\left(\frac{2}{\pi}\right) + \cos\left[\sin^{-1}\left(\frac{2}{\pi}\right)\right] - 1\right\} \approx 0.1053 \tag{11}$$

Analysis of the discontinuous mode of operation is more difficult than for CCM. While closed form solutions for the PF and its phase displacement component cannot be found, it is not hard to show that these two quantities remain functions of K_l alone. Appendix A outlines the DCM analysis.

Because PF and its phase displacement component $\cos\phi$ are functions of K_l alone in both CCM and DCM, a single plot is sufficient to show the effect of all operating conditions. In Fig.5, PF and $\cos\phi$ are plotted versus K_l on a log scale. Maximum PF is 0.90, achieved as $K_l \to \infty$. As K_l is reduced, PF falls to a value of only 0.732 at the critical point. As K_l falls below $K_{l\,\text{crit}}$, the power factor initially increases, a somewhat surprising result. As K_l falls still further, the PF decreases monotonically.

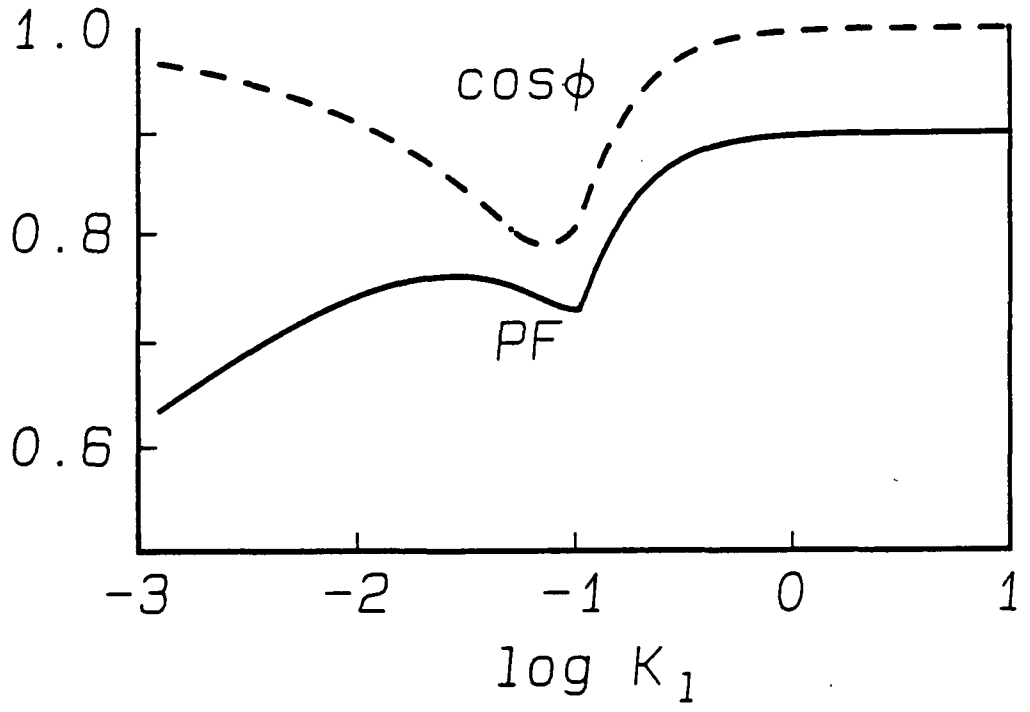

Figure 5: Power factor and its phase displacement contribution for the inductor input filter.

The curious behavior of the PF is explained in Fig.6 and the fundamental phase component plot of Fig.5. Figure 6 shows the waveshape of the line current ("unfolded" inductor current) as K_l varies. For large K_l (Fig.6(a)), the line current is nearly a square wave. The fundamental is in-phase with the line voltage; distortion alone causes the 0.90 PF limit. As K_l falls, some ripple appears across the previously flat tops of the the square wave (Fig.6(b)) and the fundamental lags slightly.

Note the discontinuities in the line current in Fig.6(a) through Fig.6(c). "Continuous conduction" of the inductor current is unrelated to the continuity of the line current. The filter must be well into discontinuous inductor current mode, with $K_l < 0.05$, before the line current becomes continuous.

Critical conduction is shown in Fig.6(c). The point where the input current reaches zero is given by Eq.(10), and is quite different from zero degrees, indicating the current is both discontinuous and out of phase. There is little distortion, but phase displacement of the fundamental keeps the PF relatively low. As K_l is reduced below its critical value, as in Fig.6(d), the distortion of the current increases, but at the same time the fundamental phase displacement decreases. The combined effect is an increase in PF. Eventually, for very small K_l, the line current becomes a narrow spike, nearly centered

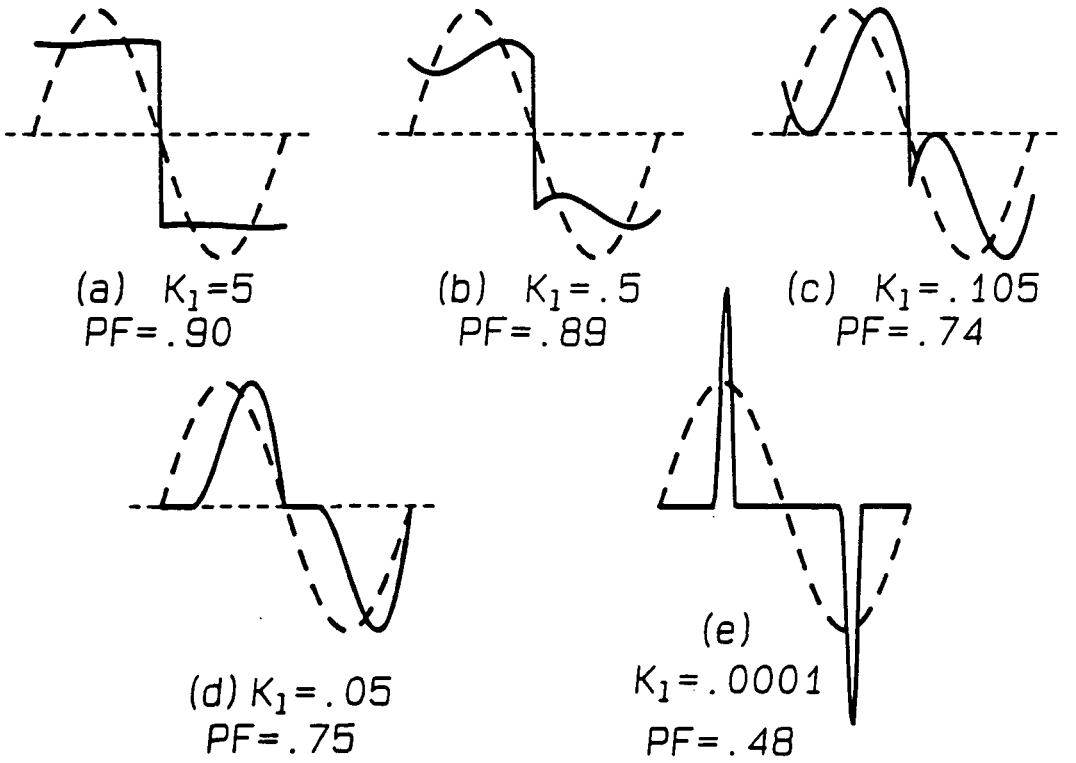

Figure 6: Line current waveforms (solid curves) for the inductor input filter as K_l changes. The dashed curves represent the line voltage. As K_l falls from a large value (a), the PF initially decreases and the phase displacement ϕ increases. Over a range of intermediate values, ((c) and (d)), PF increases and ϕ decreases with falling K_l. For small K_l (e), PF decreases with K_l and ϕ is near zero.

in the voltage half-sine, as in Fig.6(e). The fundamental is almost in phase in this case, and the low power factor is a result of distortion alone.

The inductor input filter offers the advantages of passivity, simplicity, and ruggedness. These advantages all stem from the filter containing no switches. Undesirable aspects of the filter as an input-current shaping method are the large, heavy inductor, the lack of output voltage regulation, the fact that PF varies with the load, discontinuity of the input current, and the 0.90 upper limit on PF.

3.1.2 Resonant Input Filter

Essentially unity PF *can* be achieved using only passive components. The resonant input filter, Fig.7, named by analogy with the capacitor and inductor input filters, serves as an example of this fact. Operation of this filter is easy to understand when one considers that if the Q and characteristic impedance Z_0 of the series resonant circuit are both high enough, only currents at the "notch" frequency can get through to the line, and the PF will be near unity. Analysis of the waveforms and PF is outlined in Appendix B.

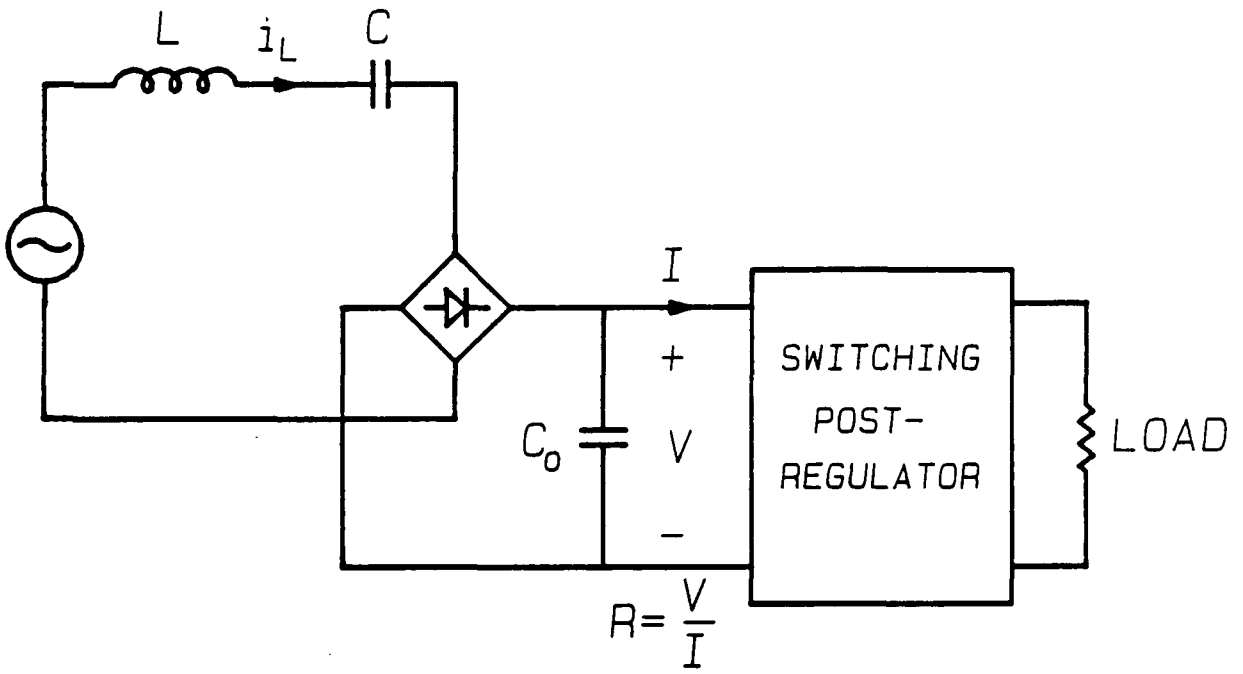

Figure 7: Resonant input filter followed by a voltage post-regulator.

As with the inductor input filter, the power factor is a function of the single parameter

$$K_l \equiv \frac{\omega L}{\pi R} \tag{12}$$

The inductance L in K_l is the resonant inductance in this case, and R is the effective load seen by the filter.

The resonant input filter has both continuous and discontinuous modes, the latter occurring when the rectifier bridge is open for some fraction of a cycle. Unlike the inductor input filter, however, the series inductance ensures that the line current is *always* continuous. Figure 8 shows the form of the input current as the parameter K_l varies. The critical value

$$K_{l\,\mathrm{crit}} = \frac{2}{\pi^2} \approx .203 \tag{13}$$

marks the boundary between CCM and DCM. The power factor as a function of K_l is shown in Fig.9. The curve is similar to that of Fig.5 for the inductor input filter, but in this case the PF is higher, 0.94 at critical conduction and approaching unity for large K_l.

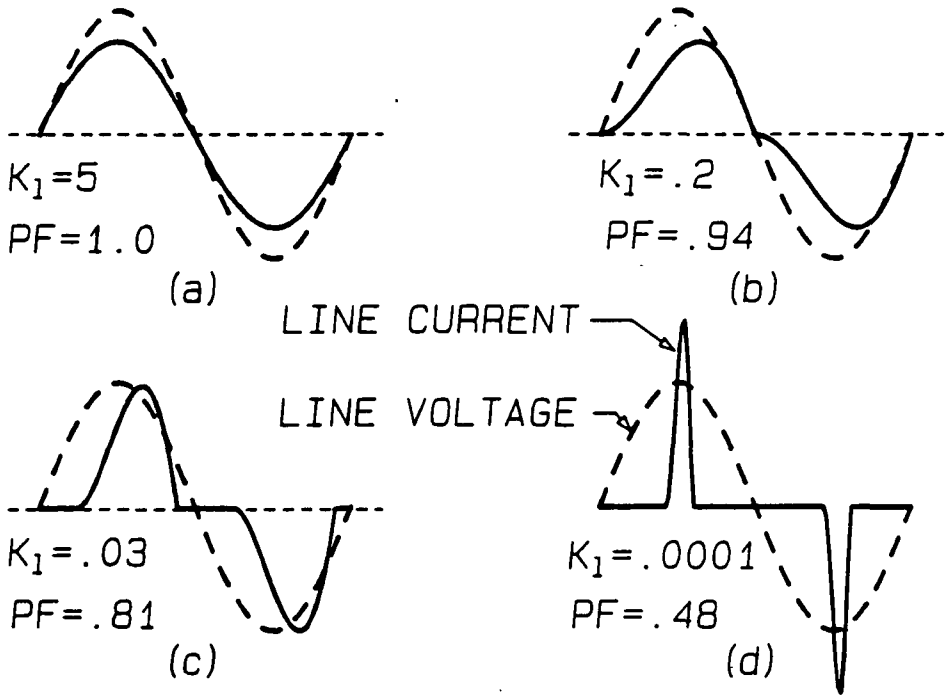

Figure 8: Line current waveforms (solid curves) for the resonant input filter as K_l changes. The dashed curves represent the line voltage. As K_l changes from a large (a) to a small value (d), PF falls monotonically, while the phase displacement ϕ initially increases, then returns to zero.

The major disadvantages of the resonant input filter are the large size of the reactive elements and the large rms current in both the capacitors. The filter is useful mainly as a demonstration that passive circuits can achieve essentially unity PF.

3.1.3 Ferroresonant Transformer

The resonant input filter is similar in some ways to the ferroresonant transformer, or ferro. Like the resonant input filter, the ferro has an L-C resonant circuit that prevents high distortion of the input current. The ferro is unique among passive methods, however, in that it uses a saturating transformer to provide some degree of regulation against input voltage changes. The ferro provides no control over the output voltage, however, so a post-regulator is still needed.

Like the resonant input filter, the ferro is heavy (as one would expect of any line frequency transformer) and is valued chiefly for its ruggedness.

3.2 Active Shaping Methods

Active devices provide a variety of ways to shape input current. Each of the basic

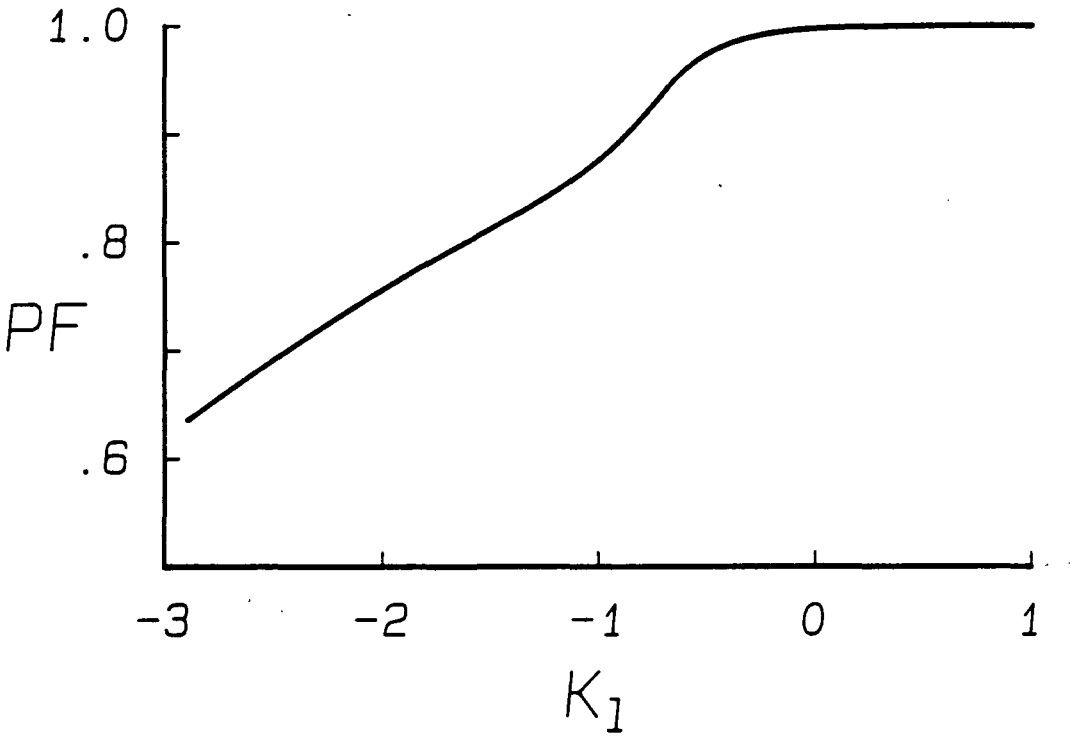

Figure 9: Power factor of the resonant input filter as a function of K_l.

ideas has several variations, leading to a bewildering number of topologies and control schemes. Despite this variety, the methods seem to fall conveniently into two categories, those based on boost-like topologies and those built around buck-related topologies. Both kinds of topologies can be operated with low switching frequencies (not more than a decade or two above the line frequency) or with fast switching. The boost topologies can operate in either a continuous or discontinuous mode, but the buck-based schemes always use continuous conduction.

3.2.1 Boost-like Topologies

The basic boost topology appears in Fig.10, shown with a bipolar switch. An inductor is placed in series with the rectified line. When the switch is on, the switch connects the end of the inductor to ground, so that the current in the inductor increases. When the switch is off, the rectifier comes on and the inductor is connected to a stiff voltage, such as a large capacitor. As long as this voltage is greater than the input voltage, the current decreases. By varying the time the switch is on, the input current can be shaped.

The boost topology is used as an example throughout this section, but other

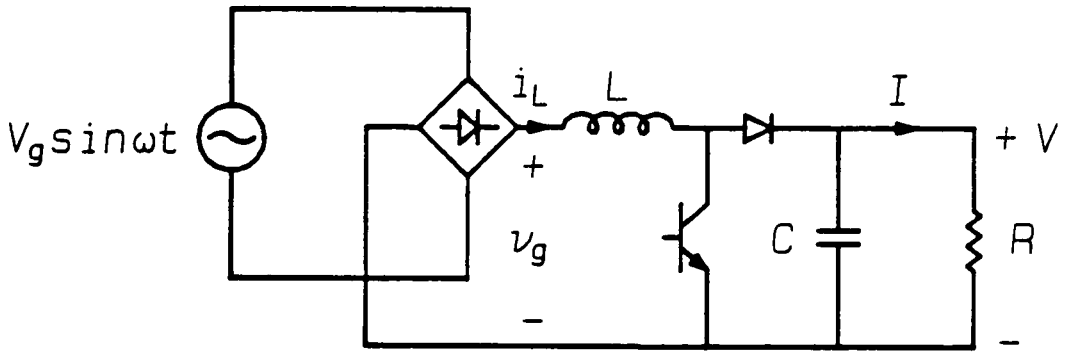

Figure 10: Boost topology.

"boost-like" topologies, such as the Ćuk and SEPIC topologies, can also be used to shape input current. In all these "boost-like" topologies, one end of an inductor is connected to the input while the other end is switched between fixed voltage levels. The inductor current, and hence the input current, is shaped by controlling the voltage applied across the inductor.

The switch in the boost topology can be operated slowly and reasonably good PF will result. Some examples of this kind of operation are presented first. When the switching frequency is much higher than the line frequency (fast switching), true sine wave current is possible, and the current shaper is called a "resistor emulator" because the line current is proportional to the line voltage. Guidelines for choosing the inductor in this case are studied next. The boost topology can mimic the inductor filter with infinite inductance by programming the inductor current to be constant. Some advantages to this scheme are discussed. Finally, the boost topology can be operated with discontinuous inductor current and constant switch duty ratio, leading to a kind of "automatic" resistor emulation mode.

Slow-switching Boost

With a switching frequency a scant 8 or 10 times the line frequency, the boost topology of Fig.10 can deliver PF's of well over 90 percent. Figure 11 shows some examples of the line current waveform. Two parameters determine the PF for a given switching frequency: the conduction parameter

$$K_l \equiv \frac{\omega L}{\pi R} \tag{14}$$

and the voltage gain V/V_g. In Fig.11, there are five constant frequency switching intervals per line cycle, and the voltage gain is 1.5.

For large K_l, Fig.11(a), the dc inductor current is large and the line current is nearly a square wave. Power factor in this case approaches 0.90, just as in the inductor input filter with large K_l. (It is interesting to note that the boost topology *is* an inductor

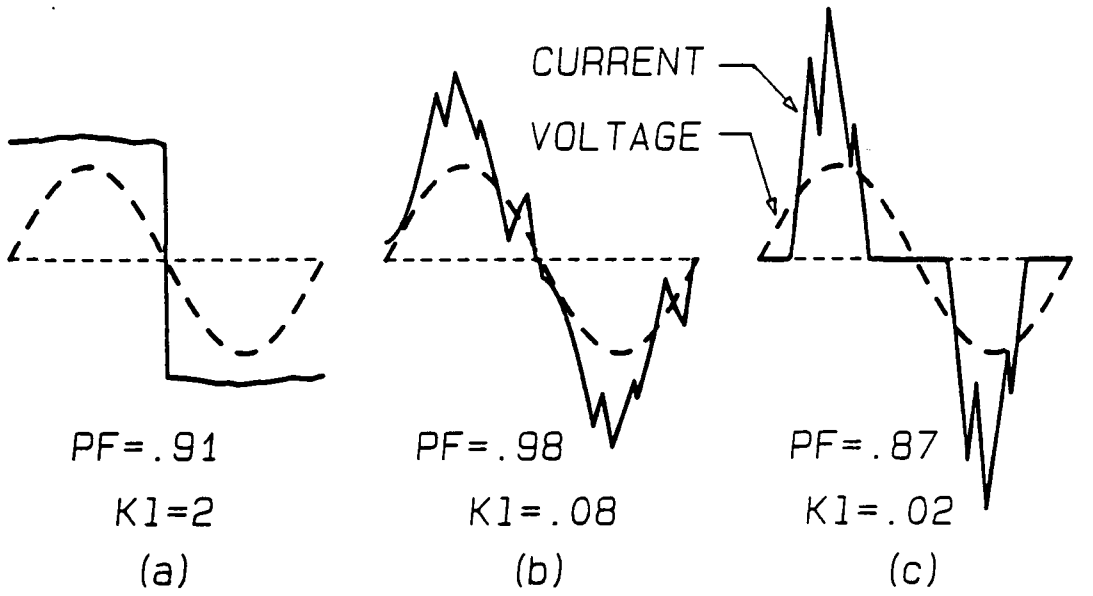

Figure 11: Line current waveforms for the boost topology switched at low frequency.

input filter if the switch is kept off indefinitely.) For decreasing K_l, the inductor current becomes more "peaky", as in Fig.11(b). For still lower K_l, the inductor current becomes discontinuous, as shown in Fig.11(c).

The input current is shaped by controlling the switching times. Power factor, or other criteria, can be optimized over these variables. A numerical multivariable optimization routine can find the best switching scheme to meet PF and harmonic distortion constraints.

In practice, specifications such as constant switching frequency and maximum or minimum on time will likely constrain the switching times. The waveforms of Fig.11(b) are for optimal PF assuming constant switching frequency and no minimum on or off time. Optimal values for the switching times change as the load and output voltage change. An optimal control scheme would therefore be complicated, probably requiring microprocessor control.

Problems with the boost topology at low frequency include high peak currents and the intelligent control needed. Line current is discontinuous at the crossover of the input voltage sine wave unless K_l is low. The fundamental of the input current tends to lag because of the difficulty in increasing the inductor current early in the cycle when the input voltage is low. Proper choice of the inductance can correct this effect at the expense of higher current peaks and lower form factor. The most important drawback, however, is the drastic change in the form of the line current as the load varies, demonstrated in Fig.11.

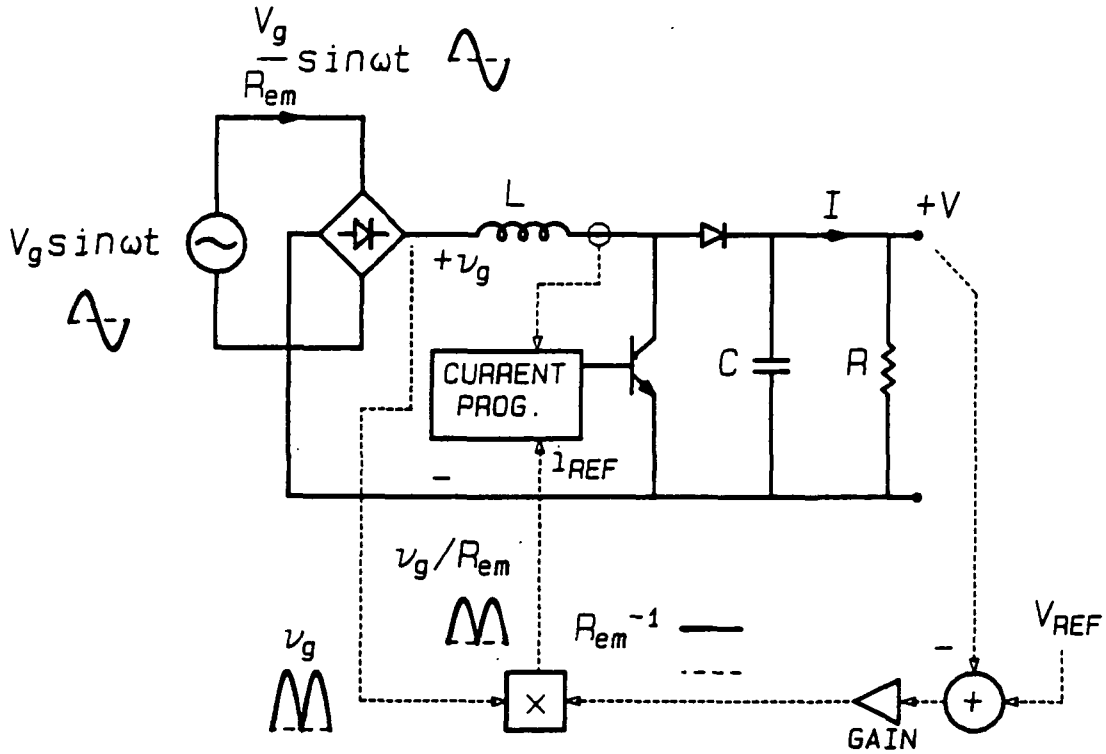

Figure 12: Control of the boost resistor emulator.

Resistor Emulator

When the boost topology operates with switching frequency well above the line frequency, the inductor current can be programmed to be proportional to the rectified input voltage [3], [4], [6]. The input current is then a sinusoid proportional to input voltage, plus some high frequency ripple. This scheme has been given the name "resistor emulator," although any input-current shaper with unity PF emulates a resistor.

Control of a boost resistor emulator is fairly simple, as shown in Fig.12 [3]. The switch is current programmed so that the inductor current closely follows some reference. An error signal, R_{em}^{-1}, generated by a voltage feedback loop, scales the input voltage to produce the reference current. The bandwidth of the voltage loop must be less than the line frequency to ensure proper current shaping (see Section 2.2).

Ideally, the switching frequency is so much higher than the line frequency that ripple effects can be ignored and averaging can be performed to study the effect of the switch. If the short-time average (switching frequency effects averaged but line frequencies remaining) of the transistor switch is $D(\omega t)$, the average voltage across the inductor is

$$v_L(avg) = v_g(\omega t) - D'(\omega t)V \tag{15}$$

where $D'(\omega t)$ is $1 - D(\omega t)$, the complement of the switch duty ratio. If the converter

emulates a resistor, the current is related to the rectified line voltage by

$$i_L(\omega t) = \frac{V_g}{R_{em}} |\sin \omega t| \tag{16}$$

where R_{em} is a constant, called the emulated resistance. The duty ratio required to generate this current waveform is found by differentiating Eq.(16), multiplying by L and equating the result to Eq.(15), yielding

$$D'(\omega t) = \frac{V_g}{V} \frac{1}{cos\gamma} \sin(\omega t - \gamma) \tag{17}$$

where γ is defined by

$$\tan \gamma \equiv \frac{\omega L}{R_{em}} = \pi K_e \tag{18}$$

Thus K_e is

$$K_e = \frac{\omega L}{\pi R_{em}} \tag{19}$$

and is analogous to the conduction parameter K_l defined earlier. The difference is that K_e involves the *emulated* resistance R_{em}, while K_l contains the effective load resistance R.

The duty ratio $D'(\omega t)$ of Eq.(17) must lie between 0 and 1. The latter constraint is satisfied when

$$\frac{V}{V_g} > \frac{1}{cos\gamma} \tag{20}$$

but the constraint that $D'(\omega t)$ be positive cannot be satisfied for ωt near zero. The physical explanation of this effect is illustrated in Fig.13. For small ωt, the input voltage is near zero. The inductor current, trying to follow the commanded current $v_g(\omega t)/R_{em}$, rises fastest with the switch on, or $D' = 0$. With the switch held continuously on, the current i_L is

$$i_L(\omega t) = \frac{1}{L} \int_0^{\omega t} V_g \sin \omega\tau \, d\omega\tau = \frac{V_g}{\omega L} (1 - \cos \omega t) \tag{21}$$

Equation (16) represents the desired current while Eq.(21) is the highest current possible for small ωt. The two waveforms converge when $\omega t = 2\gamma$; after this time the desired current waveform can be followed exactly. If the inductor current is programmed to follow Eq.(16), the actual effect will be

$$i_L(\omega t) = \begin{cases} \frac{V_g}{\omega L}(1 - \cos \omega t) & 0 < \omega t < 2\gamma \\ \frac{V_g}{R_{em}} |\sin \omega t| & 2\gamma < \omega t < \pi \end{cases} \tag{22}$$

and

$$D'(\omega t) = \begin{cases} 0 & 0 < \omega t < 2\gamma \\ \frac{V_g}{V} \frac{1}{cos\gamma} \sin(\omega t - \gamma) & 2\gamma < \omega t < \pi \end{cases} \tag{23}$$

This assumes the switch duty ratio can reach zero. In practice the minimum on time may be restricted and the time when the inductor current finally reaches the reference current will be somewhat later than $\omega t = 2\gamma$.

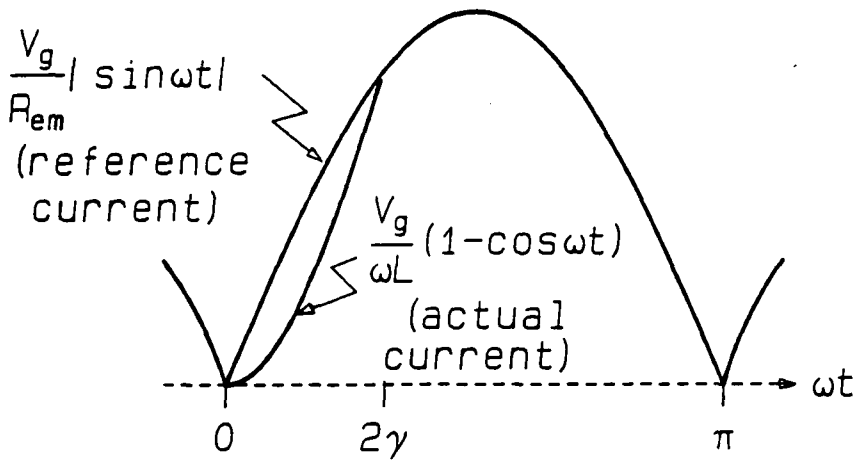

Figure 13: Distortion of the boost inductor current waveform as the reference current leaves the cusp.

This "lag" effect in the initial inductor current affects the output voltage and PF. To find the output voltage, the average output current I,

$$I = \frac{1}{\pi}\int_0^{\pi} i_L(\omega t)D'(\omega t)\,d\omega t \tag{24}$$

is evaluated using Eqs.(22) and (23), and the result multiplied by R, yielding

$$\frac{V}{V_g} = \left[\frac{R}{2R_{em}}\left(1 - \frac{2\gamma}{\pi} + \frac{1}{\pi}\sin 2\gamma\right)\right]^{1/2} \tag{25}$$

The mean square current can be found from Eq.(22) and the PF follows.

$$\mathrm{PF} = \frac{1 - \frac{2\gamma}{\pi} + \frac{1}{\pi}\sin 2\gamma}{\left\{1 - \frac{2\gamma}{\pi} + \frac{1}{2\pi}\sin 4\gamma + \frac{2}{\pi}\cot^2\gamma\left[3\gamma - 3\sin\gamma\cos\gamma - 2\sin^3\gamma\cos\gamma\right]\right\}^{1/2}} \tag{26}$$

Finding the Fourier coefficients of the odd extension of Eq.(22) into the complete line period enables the phase displacement component of PF to be calculated.

$$\cos\phi = \frac{\frac{\pi}{2} - \gamma + \frac{1}{2}\sin 2\gamma}{\left\{\left(\frac{\pi}{2} - \gamma + \frac{1}{2}\sin 2\gamma\right)^2 + \left[\cos\gamma\left(\cos\gamma - \frac{\gamma}{\sin\gamma}\right)\right]^2\right\}^{1/2}} \tag{27}$$

Equations (26) and (27) consider only the effect of the initial "lag" in the current waveform, and are independent of the switching frequency. The effect on PF of the high frequency ripple current has been studied by Rippel [4], who neglected any error at the cusp, essentially assuming $\gamma = 0$. If the two nonidealities, nonzero γ and finite switching

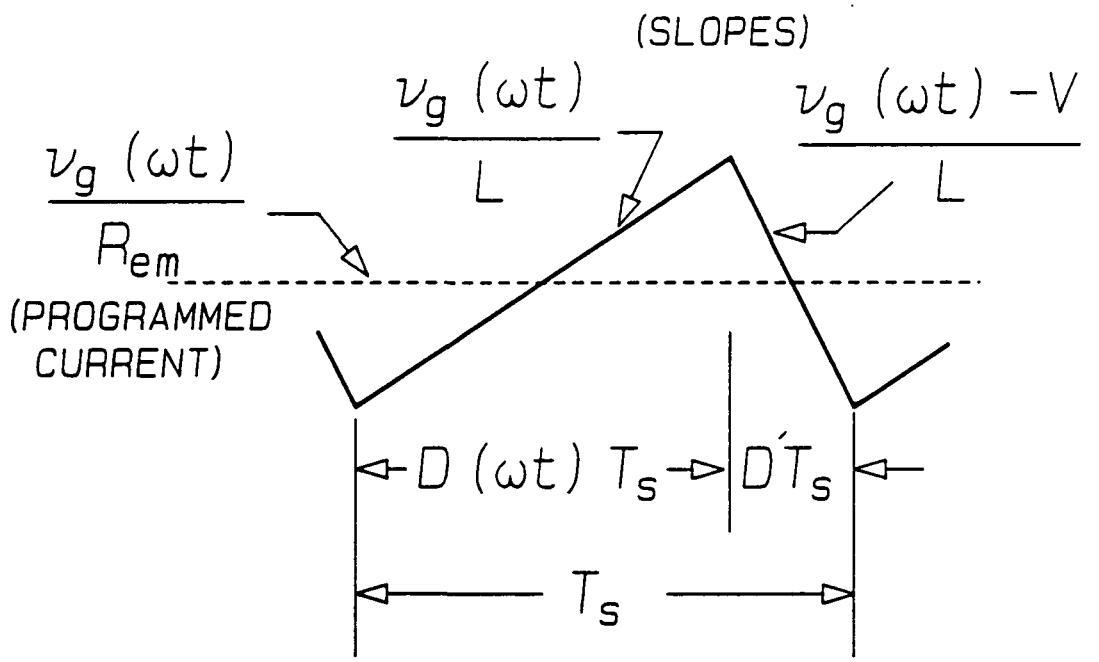

Figure 14: Switching ripple on the inductor current of the boost resistor emulator.

ripple, each cause small deviations from the ideal current waveform, one may treat the two effects separately and find the total PF as the product of the PF's derived by the separate calculations.

To evaluate the effect on PF of switching ripple alone, consider Fig.14, where the inductor current is shown over a single switching period. Again, assuming the switching frequency much greater than the line frequency, the reference current can be considered constant during any one switching cycle. The rms current contains both line frequency and switching frequency components. Since the ripple component has zero average, the total mean square current is the sum of the mean squares of the line component (ideal current waveform) and the switching ripple component (zero average triangular waveform). The peak-to-peak value of the ripple current is

$$i_{r\,p-p} = \frac{D(\omega t)T_s v_g(\omega t)}{L} \tag{28}$$

For negligible "lag" effect near the cusp, the duty ratio $D(\omega t)$ is found from Eq.(17) with $\gamma = 0$,

$$D(\omega t) = 1 - D'(\omega t) = 1 - \frac{V_g}{V}\sin\omega t \tag{29}$$

The mean square ripple current during any single switching cycle is just the peak-to-peak

value squared divided by $\sqrt{12}$, or

$$i_{r\,\mathrm{rms}}^2 = \left(1 - \frac{V_g}{V}\sin\omega t\right)^2 \frac{T_s^2 V_g^2 \sin^2\omega t}{12L} \tag{30}$$

By invoking the assumption of high switching frequency, however, the mean square ripple current can be considered a continuous function of ωt, and the total mean square ripple current is found by averaging Eq.(30) over a half-cycle of the line, to find

$$I_{r\,\mathrm{rms}}^2 = \frac{V_g^2 T_s^2}{24}\left[1 - \frac{16}{3\pi}\left(\frac{1}{M}\right) + \frac{3}{4}\left(\frac{1}{M}\right)^2\right] \tag{31}$$

where $M \equiv V/V_g$. The total mean square current is the mean square of the ideal current, $V_g^2/2R_{em}$, plus the mean square of the ripple from Eq.(31). The resulting PF is

$$\mathrm{PF} = \frac{1}{\left\{1 + \frac{1}{3K_{es}^2}\left[1 - \frac{16}{3\pi}\left(\frac{1}{M}\right) + \frac{3}{4}\left(\frac{1}{M}\right)^2\right]\right\}^{1/2}} \tag{32}$$

where K_{es} is defined by

$$K_{es} \equiv \frac{2L}{R_{em}T_s} = \frac{\omega_s L}{\pi R_{em}} \tag{33}$$

The *e* subscript refers to the dependence of K_{es} on the *emulated* resistance, while the *s* subscript indicates that it is the *switching* frequency that appears in K_{es}.

Because the ripple has zero average during each switching cycle, it adds no phase displacement to the PF. Equation (32) represents distortion alone.

In Fig.15, the two effects, Eqs.(26) and (27), and Eq.(32), are plotted against K_e on a log scale. Since $K_{es} = (\omega_s/\omega)K_e$, the curve showing the ripple effect is shifted relative to the lag effect curve as the switching frequency changes. Figure 15 shows the relationship of the two PF components for $\omega_s = 1000\omega$. For lower switching frequency, the ripple curves move to the right, defining a more narrow region where the PF is near unity. For higher switching frequency, the ripple curve moves to the left and a broader range of K_e values (inductance values) give acceptable PF. When the total PF is near 1, it may be found by multiplying together the individual PF's resulting from ripple and lag alone. If either effect is large, treating the two separately is not such a good approximation. At any rate, Fig.15 shows how the inductance L must be chosen in terms of the load and switching frequency if near-unity PF is needed. Alternatively, if the acceptable switching ripple (and hence K_{es}) is specified, Fig.15 shows the necessary separation of the line and switching frequencies to obtain a specified PF.

Both [3] and [4] show that the inductor current goes discontinuous near the cusp if $K_{es} < 1$. This is frequently taken as a lower bound for acceptable current ripple.

Constant Current Mode

An interesting way to use the boost topology is to program the inductor current to be constant. The effect is that of an inductor input filter with $L \to \infty$, so that the PF approaches 0.90. The difference is that in the inductor input filter with PF near 0.90, a large inductor is required and the filter capacitor can be small. With constant current in

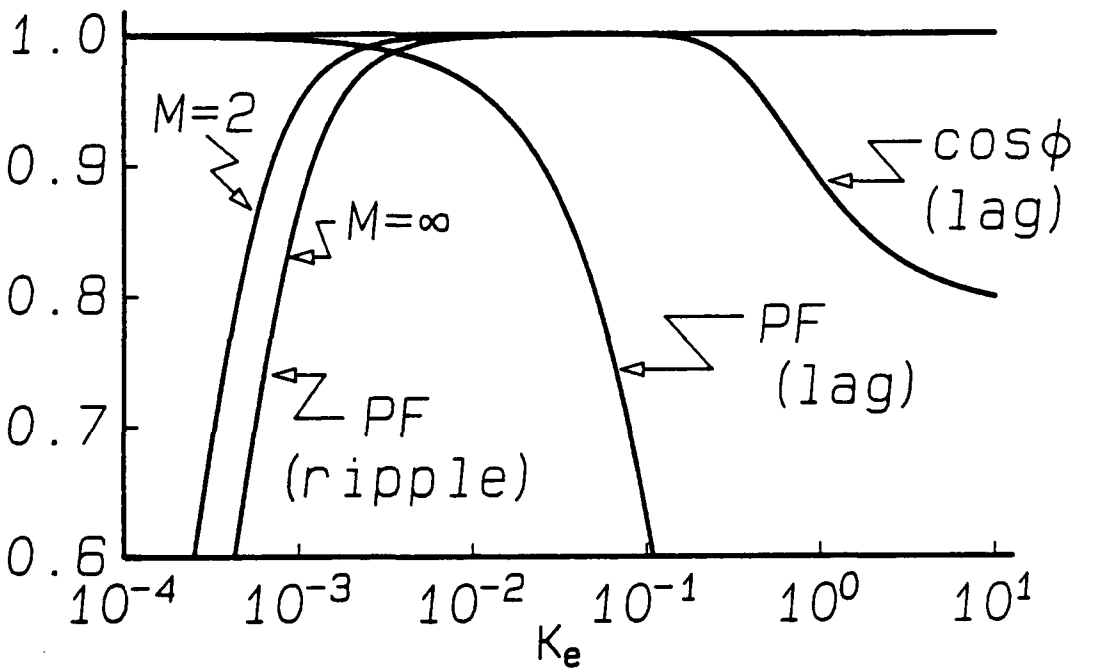

Figure 15: Power factor of the boost resistor emulator, considering both "lag" effects following the cusp and switching frequency ripple.

the boost topology, the inductance can be small if the switching frequency is high, and the capacitor is large instead. Since capacitors are volumetrically more energy efficient, the boost with constant current might have a weight or volume advantage. In addition, the boost provides active current limiting and output voltage regulation, features missing with the inductor input filter.

Discontinuous Conduction Mode

The boost topology offers one further mode of operation. If the switch duty ratio is kept *constant*, and the inductor current is discontinuous during every switching period, then the average of the input-current pulse in each cycle is roughly proportional to the input voltage. By filtering the input-current pulses, the line current is made proportional to the line voltage and the converter has near-unity PF [5].

To find the PF for this mode of operation, consider the boost converter of Fig.10 when the inductor current is discontinuous. The inductor current during a typical switching cycle is shown in Fig.16. The on time of the switch is fixed at DT_s. While the switch is on, the inductor current rises with a slope determined by the rectified line voltage $v_g(\omega t)$. The output voltage V and $v_g(\omega t)$ together determine the falling slope of the inductor current when the switch is off. Assuming that the switching frequency is much greater than the line frequency permits two approximations. First, the input voltage v_g can be considered constant during any single switching cycle. Second, the time interval D_2T_s can be treated as a low frequency, continuous variable by averaging over each switching cycle. With these assumptions, the time required for the inductor current to fall to zero

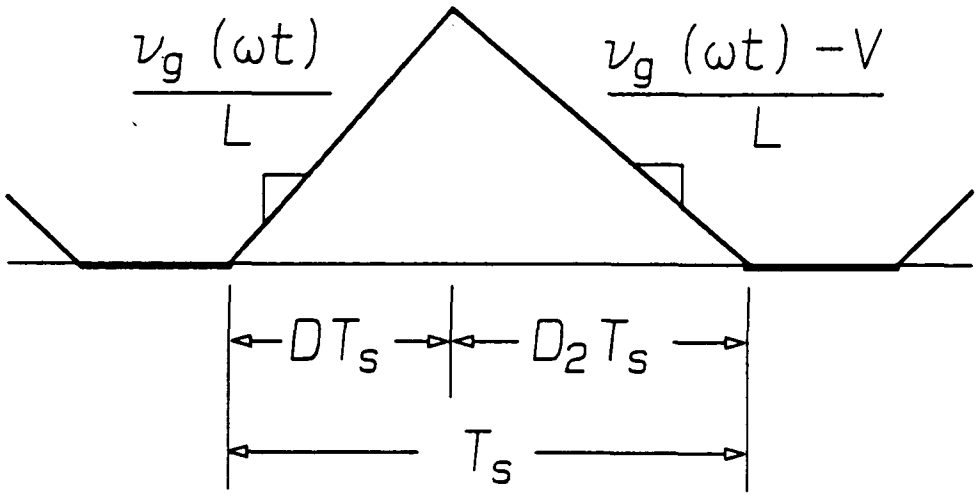

Figure 16: Inductor current of the boost topology in DCM.

is

$$D_2T_s(\omega t) = \frac{v_g(\omega t)}{V - v_g(\omega t)} D \tag{34}$$

The inductor current is discontinuous if $DT_s + D_2T_s$ is always less than T_s. Discontinuous operation is ensured throughout the line cycle if

$$D < 1 - \frac{V_g}{V} \tag{35}$$

The average inductor current during a single *switching* period is

$$i_L(\omega t) = \frac{D^2T_sV_g}{2L}\left(\frac{\sin\omega t}{1 - \frac{1}{M}\sin(\omega t)}\right) \tag{36}$$

where M is the voltage gain V/V_g. Under the assumption that an input filter removes switching ripple leaving only the line frequency part of the unfolded inductor current, i_L can be treated as a continuous variable. The input power is calculated by integrating the product of v_g and i_L, yielding

$$P_{in} = \frac{V_g^2D^2T_s}{2L}\frac{1}{\pi}\int_0^{\pi}\frac{\sin^2\omega t}{1 - \frac{1}{M}\sin\omega t}\,d\omega t \tag{37}$$

The rms line current equals the rms inductor current, the average of the square of Eq.(36),

$$\frac{1}{\sqrt{2\pi}}\frac{D^2T_sV_g}{2L}\int_0^{\pi}\frac{\sin^2\omega t}{\left(1 - \frac{1}{M}\sin\omega t\right)^2}\,d\omega t \tag{38}$$

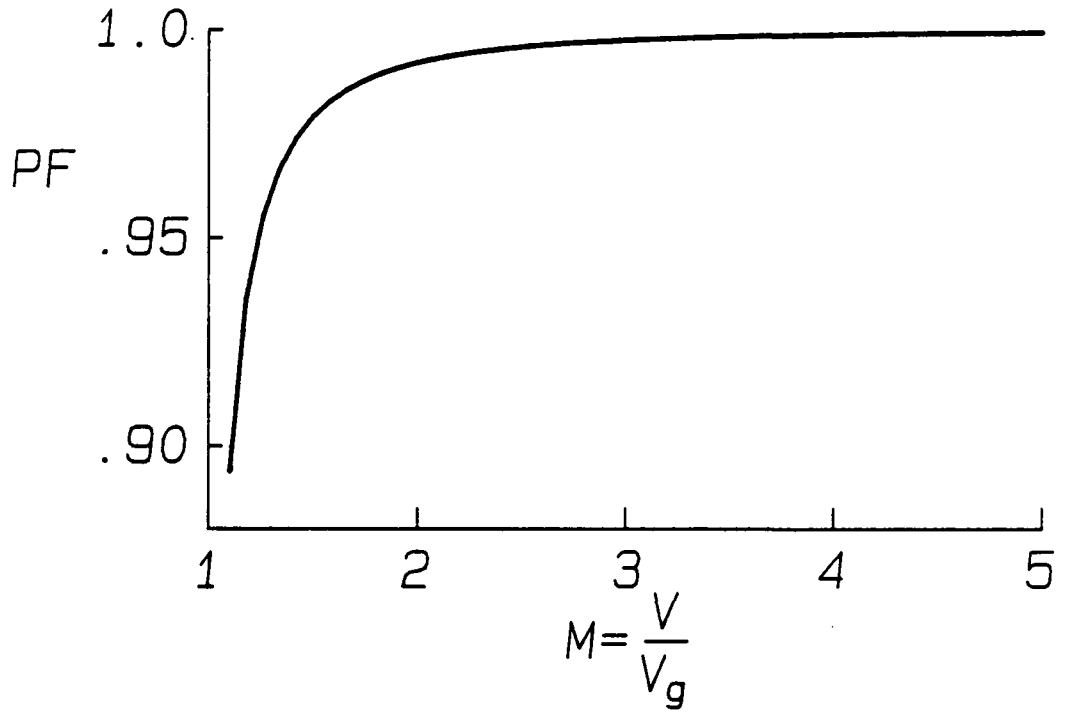

Figure 17: PF of the boost topology in DCM, neglecting switching ripple effects.

The PF can now be calculated using Eqs.(37) and (38), yielding

$$\mathrm{PF} = \sqrt{\frac{2}{\pi}} \frac{\int_0^{\pi} \frac{\sin^2 \omega t}{1-\frac{1}{M}\sin \omega t}\, d\omega t}{\left(\int_0^{\pi} \frac{\sin^2 \omega t}{\left(1-\frac{1}{M}\sin \omega t\right)^2}\, d\omega t\right)^{\frac{1}{2}}} \tag{39}$$

The integrals in Eq.(39) are apparently not available in closed form. Numerical integration can be used to evaluate Eq.(39), resulting in the PF plot of Fig.17. Because of the symmetry of Eq.(36) within a half cycle of the line voltage, there is no phase displacement. Equation (39) represents distortion alone.

The voltage gain as a function of D and the load R can be found by calculating the average output current and using $V = IR$, but the result is an implicit equation in M. For $M > 1.5$, however, the voltage gain is very nearly

$$M \approx \frac{D}{\sqrt{2K_s}} \tag{40}$$

where K_s is defined by

$$K_s \equiv \frac{2L}{RT_s} = \frac{\omega_s L}{\pi R} \tag{41}$$

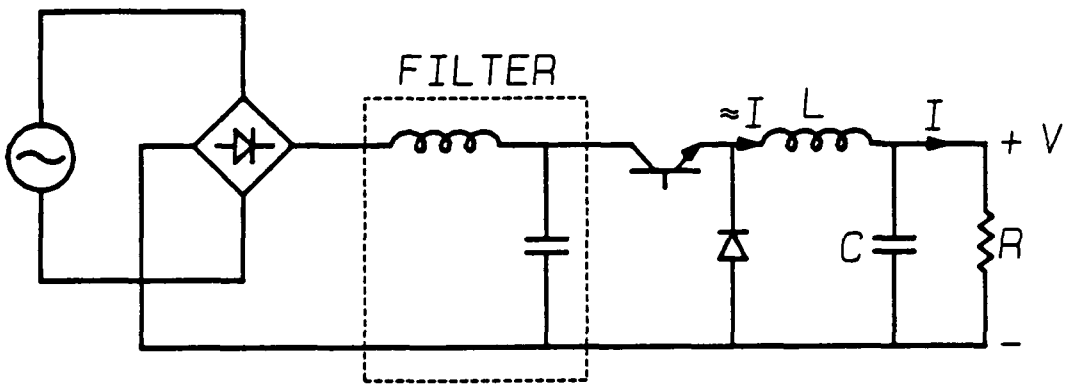

Figure 18: Buck topology.

The obvious advantage to this input-current shaping scheme is that the shaping takes place "automatically," and no current sensing or programming is required. (The voltage control must still have low bandwidth, however, to avoid disturbing the input-current shape.) The inductor current in DCM contains more high frequency noise than in the fast-switching resistor emulation mode, requiring a larger filter. The size of the filter is still dependent only on the switching frequency, however, not on the line frequency.

3.2.2 Buck-like Topologies

Another set of topologies is the buck-like group. Instead of having a series inductor switched between voltages, buck-like converters have a constant current source that is alternately connected to the input and shunted to ground. In addition to the basic buck converter, any of the buck-derived topologies, including half- and full-bridge versions, can be used as input-current shapers. The buck-boost, or flyback, topology is another buck-like topology with the potential for current shaping. Figure 18 shows a buck topology using a large inductor for the source of constant current. Buck topologies switched at low frequencies usually use a controlled bridge, as in Fig.19, rather than a rectifier bridge and separate control switch. The input current is made up of chops of the constant current source. When switched at relatively low frequencies, buck current shaping methods are known collectively as "pulse-width-modulation," or PWM.

A filter should be used with buck-like topologies to prevent the discontinuous input current from reaching the line. Unity PF is impossible without such a filter.

One major difference between boost and buck-like topologies is the form of the energy storage. Boost topologies store energy in a source of constant voltage, such as a large capacitor. The buck-like methods store energy in a current source, such as a large inductor. Filtering the discontinuous input current still requires a capacitor handling high rms currents, though the capacitance value can be low. Another difference is that boost converters have output voltages *greater* than the peak of the line voltage, and switching transistors see this voltage. Buck converters provide output voltages *lower* than the line

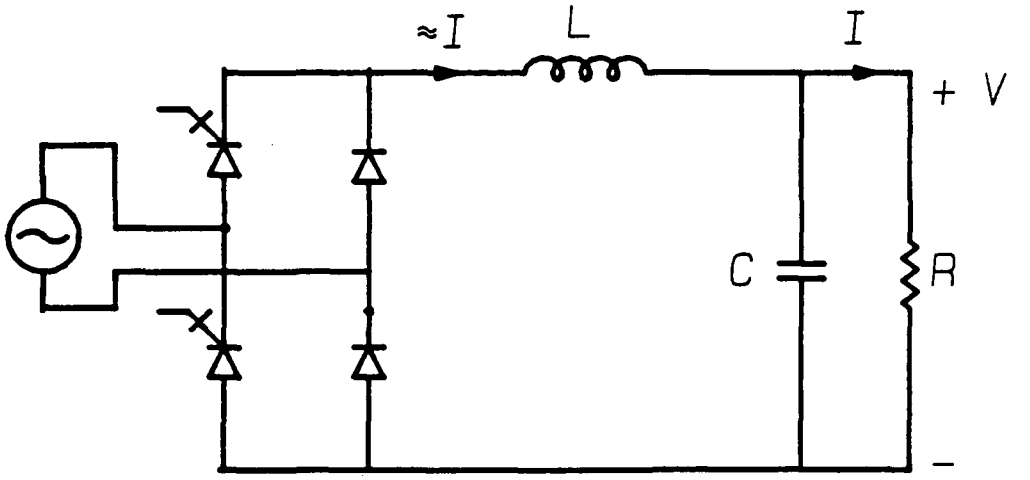

Figure 19: Buck topology with controlled bridge for high power applications.

voltage, and the switches need only handle the peak line voltage.

Resistor Emulator

When the switching frequency is very far above the line frequency, the buck topology can achieve unity PF and emulate a resistor, like the boost topology. In the case of the buck, the average input current is the switch duty ratio times the constant inductor current. By varying the duty cycle of the switch, any value of average current from zero to the constant current value can be drawn from the line. A filter ensures that the line sees only the short-time average of the chopped current, rather than the chopped waveform itself with its high frequency content. The size of the filter diminishes with the switching frequency, and is independent of line frequency. An example of a buck-like topology switched at high frequency is found in [9], where a flyback topology is used.

The buck topology itself has no problem following the cusp of the desired input-current waveform, but addition of a filter at the input will introduce di/dt limits, producing some error at the cusp. As in the boost topology, a large separation of the line and switching frequencies makes it possible to adequately filter out high frequency ripple while still having small errors near the cusp.

Current programming is the natural choice for control in a *boost* resistor emulator because the input current appears in the inductor and in the transistor during the on time. In the buck topology, however, the actual input current is discontinuous and cannot be programmed.

Sawtooth Modulation

Low frequency PWM methods have two main features: where the switching instants are placed within the line period, and how the actual switching is accomplished. For high power schemes, the latter usually involves commutation of SCR's. For a given

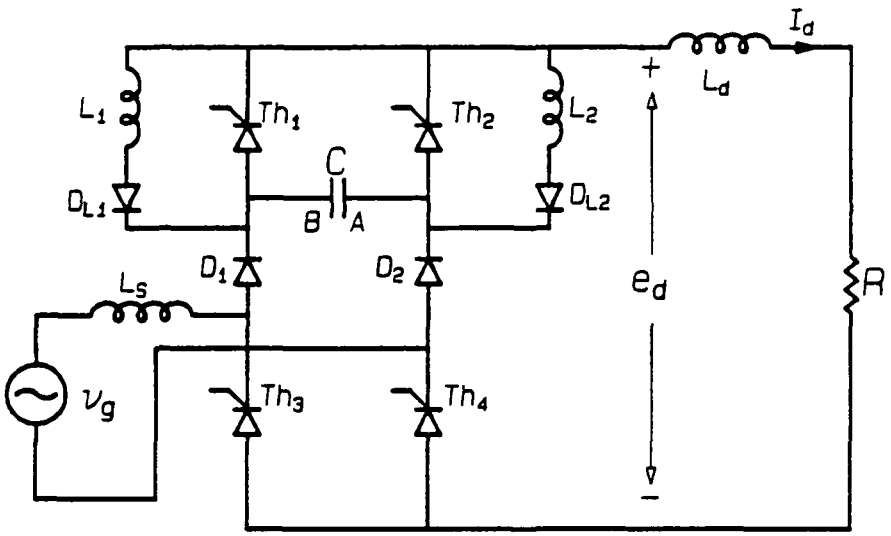

Figure 20: Topology used in the "sawtooth" modulation scheme.

number of switching transitions per line cycle, the transitions can be placed to satisfy some criteria of optimality, such as high PF or reduction of specific harmonics.

Among the many low frequency PWM schemes, one known as sawtooth modulation is unusual in that it requires no extra thyristors for commutation [10]. Sawtooth modulation uses the circuit of Fig.20. To understand the operation, assume thyristor Th_1 is on and the commutating capacitor C has terminal A positive and B negative. When thyristor Th_2 is turned on, the capacitor voltage reverse biases and turns off thyristor Th_1.

The capacitor C discharges through L_1, D_{L1} and the load and reverses the polarity until D_1 clamps the supply voltage and D_2 begins to conduct. L_s is included to boost the voltage on capacitor C when the line voltage is near zero, in order to ensure successful commutation in the next cycle.

Figure 21 shows the modulation scheme used in sawtooth modulation. The gate signals for the thyristors are obtained by comparing a triangular voltage e_t with a rectified sinusoidal voltage e_s synchronized with the line voltage. Output voltage regulation is achieved by varying the amplitude of e_s, or the ratio $e_{s\,max}/e_{t\,max}$.

4 Energy Storage Methods

As discussed in Section 2.1 above, all resistor emulators must store a minimum amount of energy, regardless of their switching frequency. Whether a boost-like or buck-like input is used, the converter can store energy in several ways, as illustrated by the

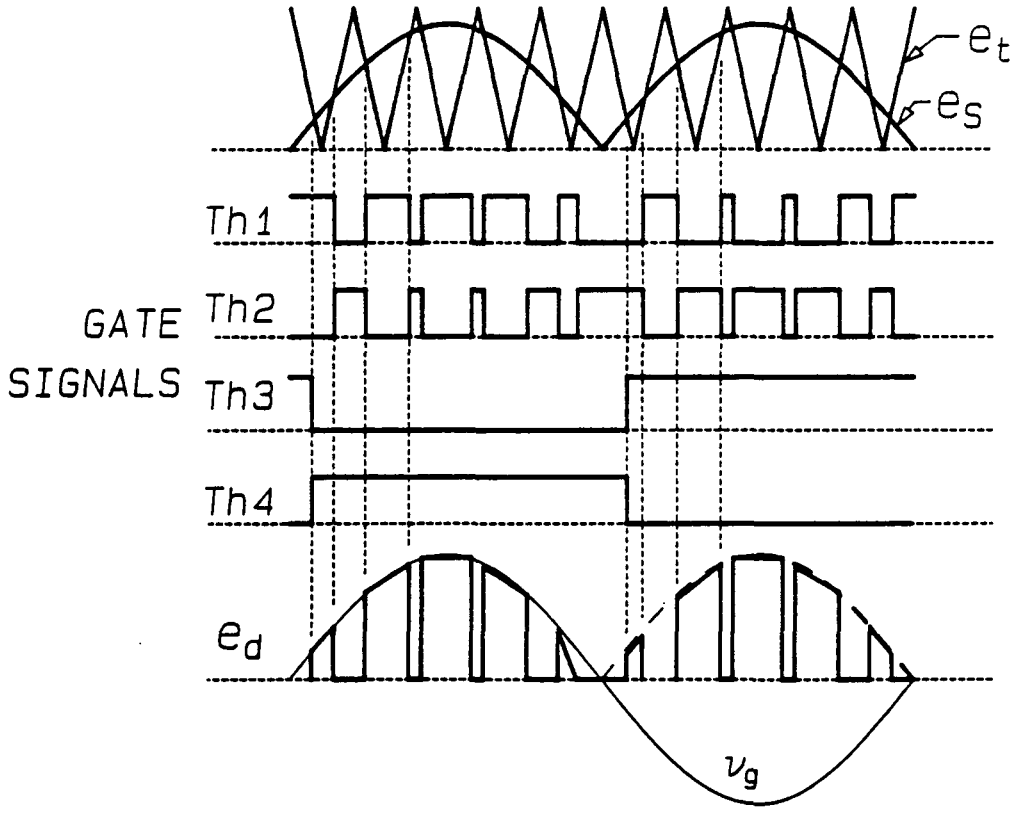

Figure 21: Control method used in sawtooth modulation.

methods described in the sections below.

Despite the high costs of extra stored energy, it is not always desirable to store only the minimum energy required by power balancing. A common specification for off-line converters is a minimum hold-up time, a requirement that calls for a large amount of stored energy. Using a large capacitor in a boost resistor emulator, for example, is not a waste of size and weight if the extra energy is needed for hold-up. Another use of extra stored energy is meeting sudden changes in load demand. Suppose a minimum-energy scheme is being employed and a sudden increase of load power is called for when the stored energy is at its minimum. Since the converter stores no energy at this instant, the increase in load power can only come directly from the line. The line current amplitude is only allowed to change slowly, however, as discussed in Section 2.2. Even if the line current could be changed quickly, the presence of reasonably large capacitors or inductors in the power processor makes it impossible to rapidly change the state of the converter and increase the load power. The minimum energy stored in a current-shaping power processor must be such that load changes and hold-up specifications can be met during any portion of the line period.

4.1 Large Reactance

The simplest way to store energy under nearly constant voltage or current is to use a large capacitor or inductor, respectively. In the boost converter, for example, a large output capacitor is used to hold the output voltage constant, as in Fig.10. The current through this capacitor is a sinusoid at twice the line frequency. The capacitor takes up and releases energy to account for the difference between input and output power. The peak energy stored in the capacitor is much greater than that required by theoretical power balancing, however, because of the large capacitance necessary to keep the ripple voltage small while a large sinusoidal current flows.

An energy storage capacitor will have a large rms ripple current at the line frequency. In addition, if a switching converter is used to actively shape the input current, the capacitor will also have large rms currents at the switching frequency. Large rms current capability and high capacitance in the same package means a very large and expensive capacitor. An alternative would be to use two capacitors in parallel, one of large capacitance to handle the line frequency current, and another of small capacitance to absorb the switching ripple. In either case, the energy storage capacitor will be expensive.

The inductor in buck-like converters plays the same role as the capacitor of the boost converter, maintaining its current constant while under a sinusoidal voltage. The high rms currents in the boost capacitor correspond to high rms voltages across the inductor in the buck topologies. The switching frequency rms voltage on the inductor is not a major stress, unlike the case with the boost capacitor. Buck-like topologies do not entirely avoid the rms current problem, however, because they require an input filter, and this filter must include a capacitor with large, high frequency rms current.

4.2 Active Filter

A power amplifier can effectively multiply the value of a capacitance or inductance, producing the same ripple performance as a much larger reactance alone. The "super-capacitor" filter [8] is an example of this technique. A fast-switching inverter (power amplifier) and small capacitor C_s can replace the large capacitor in a boost current-shaper, as in Fig.22. If the voltage gain of the power amp is F, the ripple voltage $\hat{v}_{rc}$ on C_s is $(1+F)$ times the ripple at the output, $\hat{v}_r$. The ripple current $\hat{i}_r$ generated by current shaping is absorbed by the filter at the lower ripple voltage. While the impedance of the capacitor is $Z_C = \hat{v_{rc}}/\hat{i}_r$, the apparent impedance seen by the load is

$$\frac{\hat{v}_r}{\hat{i}_r} = \frac{1}{1+F}\frac{\hat{v_{rc}}}{\hat{i}_r} = \frac{1}{1+F}Z_C \tag{42}$$

This assumes the power amp input current is negligible, a good approximation when

$$F\frac{\hat{v}_r}{V} \ll 1 \tag{43}$$

A small capacitor C_s therefore simulates a much larger capacitance $(1+F)C_s$, yet the peak voltage on C_s is still approximately V. The active filter thus stores less energy than a capacitor alone for a given ripple performance.

The drawback of the active filter is, of course, the expense of the power amplifier. The amplifier must be fast-switching and have a four quadrant output.

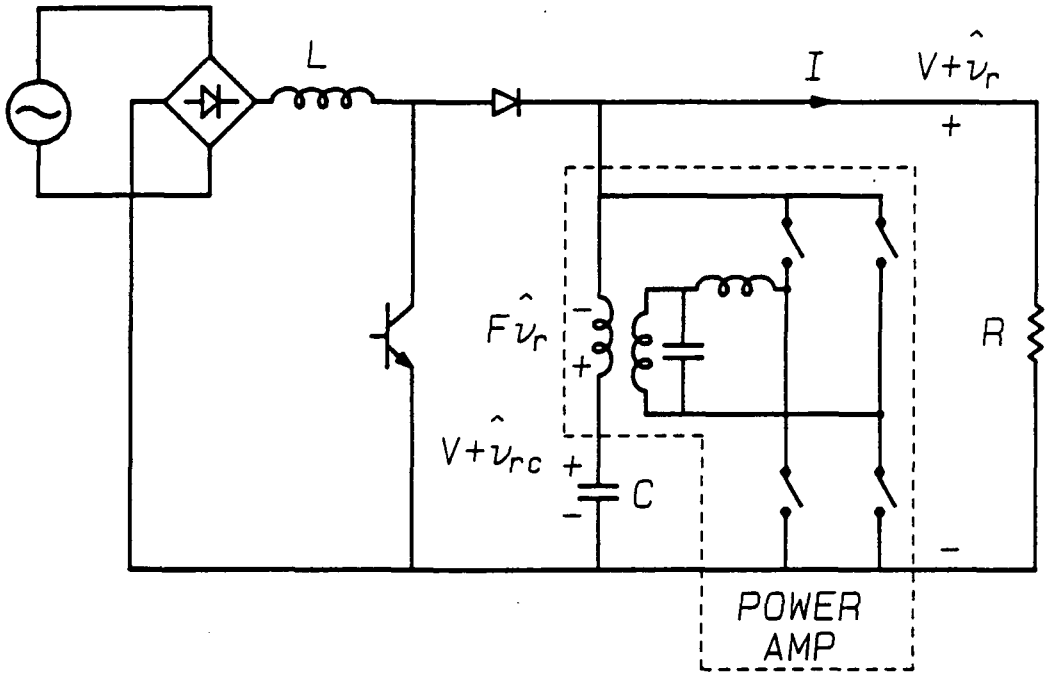

Figure 22: Super-capacitor filter in a boost current shaper.

4.3 Resonant Filter

For fast-switching current shapers with near-unity PF, an alternative form of energy storage is the resonant filter, shown in a boost resistor emulator in Fig.23 [11]. Since the short-time average of the current in the capacitor of a boost resistor emulator is sinusoidal, a resonant filter tuned to twice the line frequency will present a low impedance to the current, providing small voltage ripple. The resonant capacitor C_r must see the same dc voltage as the single capacitor it replaces, but the capacitor in the resonant filter can be much smaller for the same output voltage ripple. The capacitor C_{hf} is necessary because switching makes the actual current in the filter discontinuous and a path must be provided around the resonant inductor to allow the high frequency components of the filtered current through. A resonant filter can store as little as 1.2 times the minimum energy required for power balancing while still providing arbitrarily small voltage ripple.

Energy storage for a buck topology is the dual case of that for a boost. For a fast-switching buck resistor emulator, a parallel resonant filter can replace the main inductor, gaining the same advantages of less total stored energy.

4.4 Active Control of Energy Storage

A recent approach confronts the energy storage problem directly, choosing a topology and control scheme with the purpose of balancing the difference between input

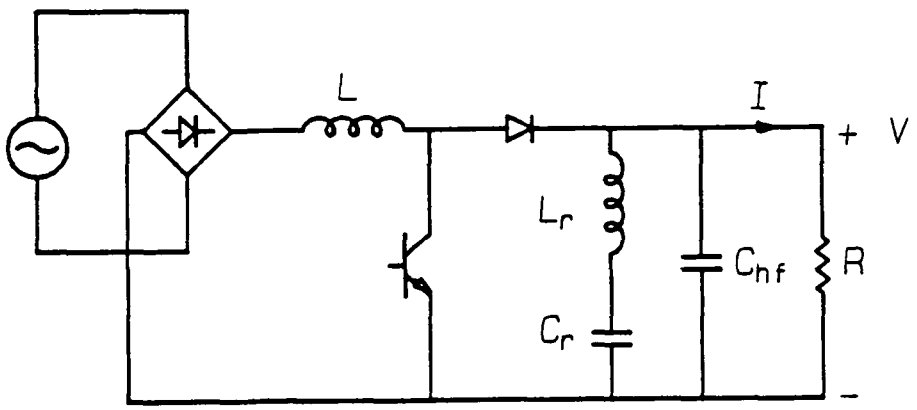

Figure 23: Resonant filter in a boost current shaper.

and output power [12]. An example of the proposed technique is shown in Fig.24. The converter can be viewed as a boost topology followed by a buck regulator. The inductor L_1 is "small", as in the boost resistor emulator, and stores insignificant energy if the switching frequency is far above the line frequency. Capacitor C_1 provides the line frequency energy storage. Stored energy in this capacitor is "programmed" in the sense that its voltage is controlled to provide energy $\frac{1}{2}C_1V^2$ that will balance the difference between instantaneous input and output power with very little extra stored energy. The time-varying voltage across C_1 is regulated by the buck post-converter so that the load voltage is dc. In theory, the capacitor voltage can vary to provide ideal energy storage while the switches on either side provide ideal input and output waveforms. To obtain precisely the theoretical minimum stored energy, the switch duty cycles must reach extreme values of 0 or 1, and the voltage across C_1 (and hence the switch voltage stresses) must be arbitrarily large. Near-ideal operation brings very good results, however. For instance, if the duty ratios are allowed a full range from 0 to 1 and the switch stresses are 1.6 times the peak line voltage V_g, then the peak stored energy is only 1.25 times the theoretical minimum. For stresses equal to V_g, the peak stored energy is twice the ideal value.

The converter offers low stored energy at the expense of some added complexity, large range of switch duty ratios, and increased voltage stress.

5 Three Switched-Network Topologies

Fast control of the output voltage in a current shaper requires more than one switch, as seen in Section 2.2. One way to introduce the extra degree of control is to follow the current shaper with a separate dc-to-dc converter. Another way is to add a

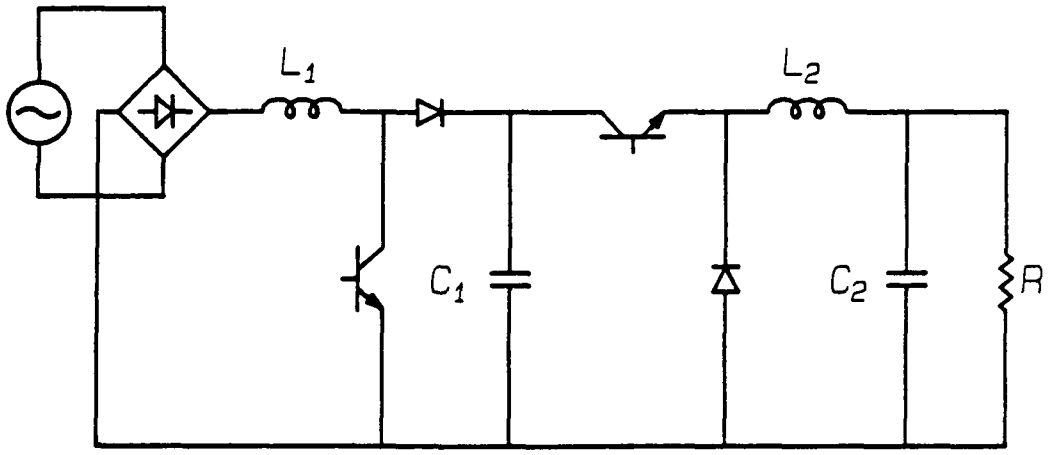

Figure 24: Topology used for directly controlling energy storage.

switch directly to the shaper topology. The resulting converter is called a three switched-network (3SN) converter [7]. Figure 25 shows an extra switch and rectifier added to a buck-boost input-current shaper (a buck-like topology). The duty ratio of the first switch is modulated to obtain the desired input current. The amplitude of the average input current and the dc inductor current are slowly regulated by the depth of this duty ratio. The added switch effectively forms a boost converter, regulating the amount of the inductor current that is fed to the load. The second switch can be dedicated to controlling the output voltage, and the response to disturbances in the output voltage can be very fast. The bandwidth of the voltage control loop depends upon the switching frequency, not the line frequency. The voltage loop can reject ripple on the main inductor, allowing a slightly smaller inductor to be used.

A switch can also be added to the Ćuk converter (a boost-like current-shaping topology) to get a current shaper with independent voltage control (Fig.26). This converter is very similar to the topology of Fig.24. Because of the extra degree of regulation afforded by the extra switch in Fig.26, the voltage on capacitor C can have large ripple. In the limit, the capacitor voltage can be varied to control the stored energy, as in Section 4.4.

The basic boost and buck topologies cannot be turned into 3SN converters, because the main energy storage element is directly connected to the output at all times.

The 3SN versions of the buck-boost and Ćuk converters have the advantage of easy isolation. In the buck-boost, the main inductor becomes a coupled inductor, as in Fig.27. The coupled inductor needs a large gap because it provides the main (line frequency) energy storage. In the Ćuk converter, addition of a transformer and an extra capacitor generates the isolated version of Fig.28. Here the transformer sees only the switching frequency and is excited in both directions, so it can be quite small. The main energy storage is in the two capacitors on either side of the transformer.

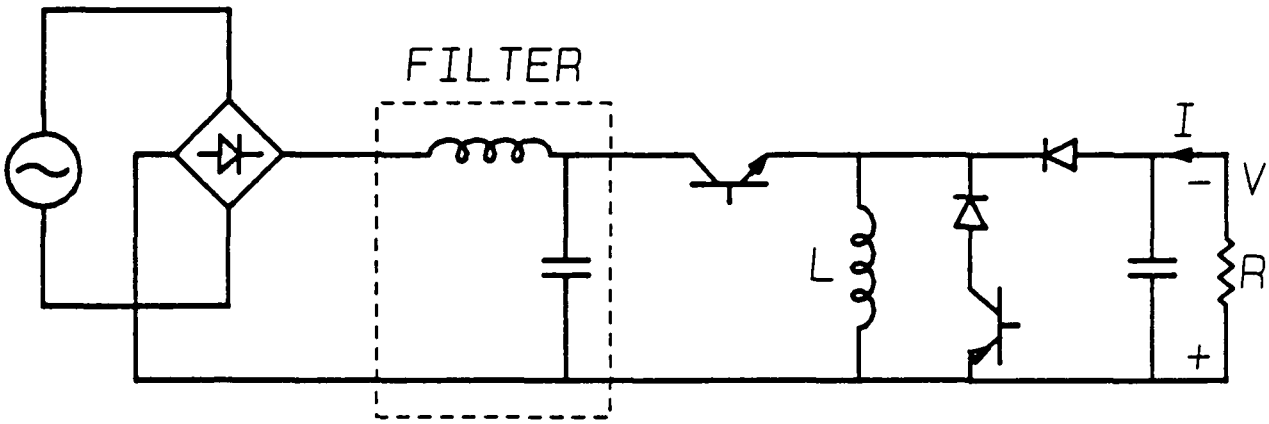

Figure 25: Three switched-network buck-boost converter.

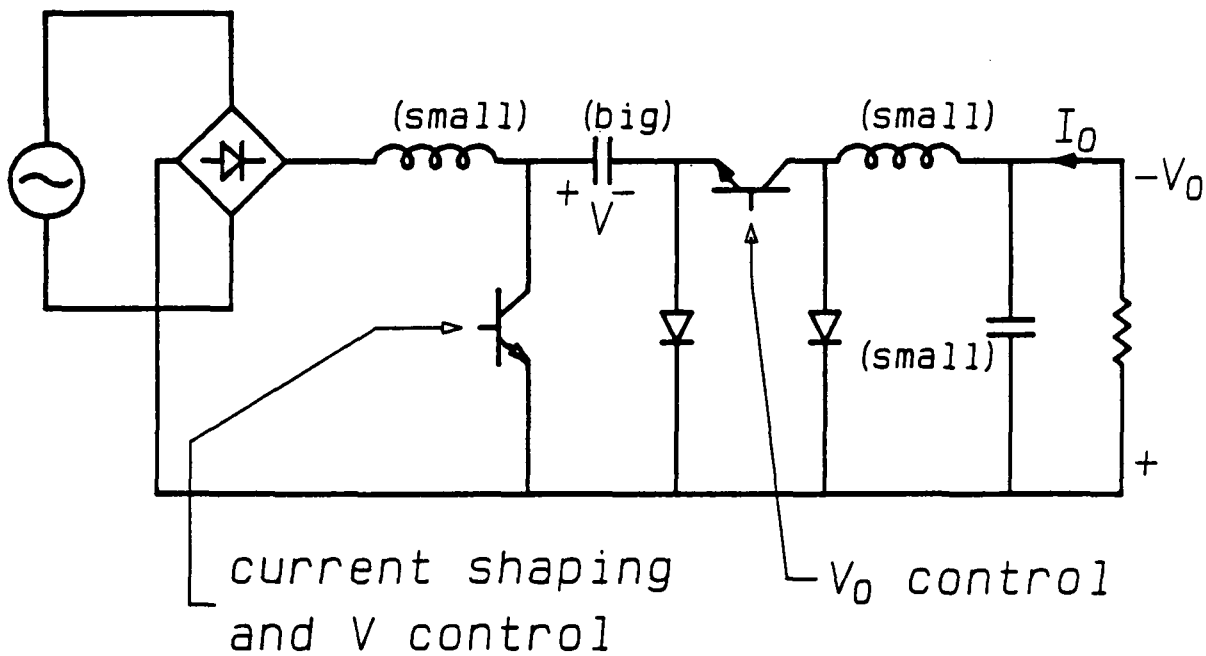

Figure 26: Three switched-network Ćuk converter.

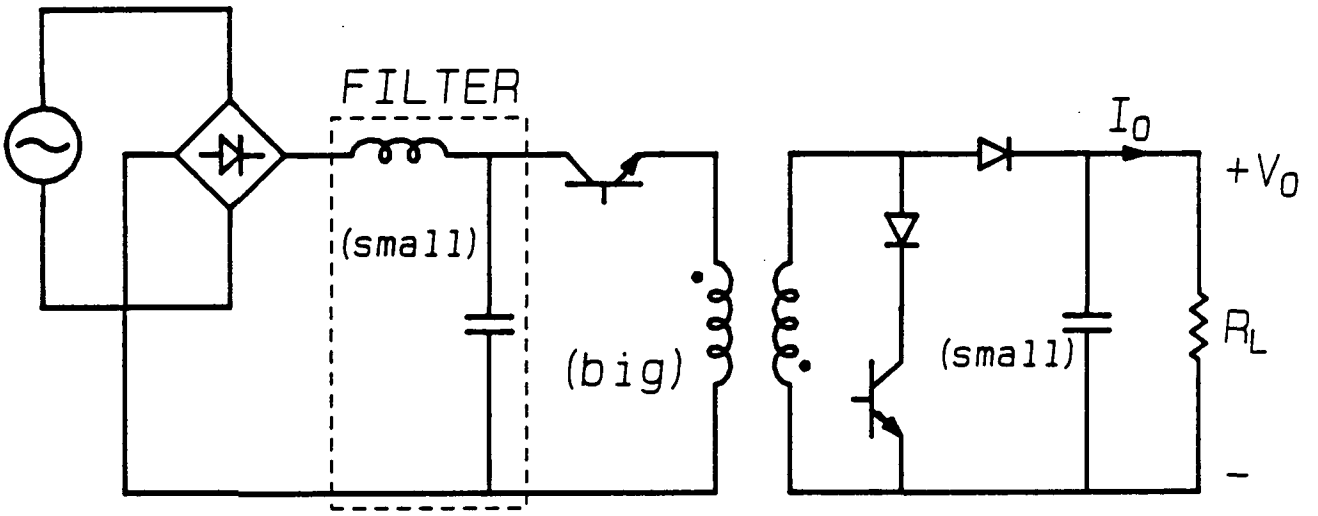

Figure 27: Isolated 3SN buck-boost topology.

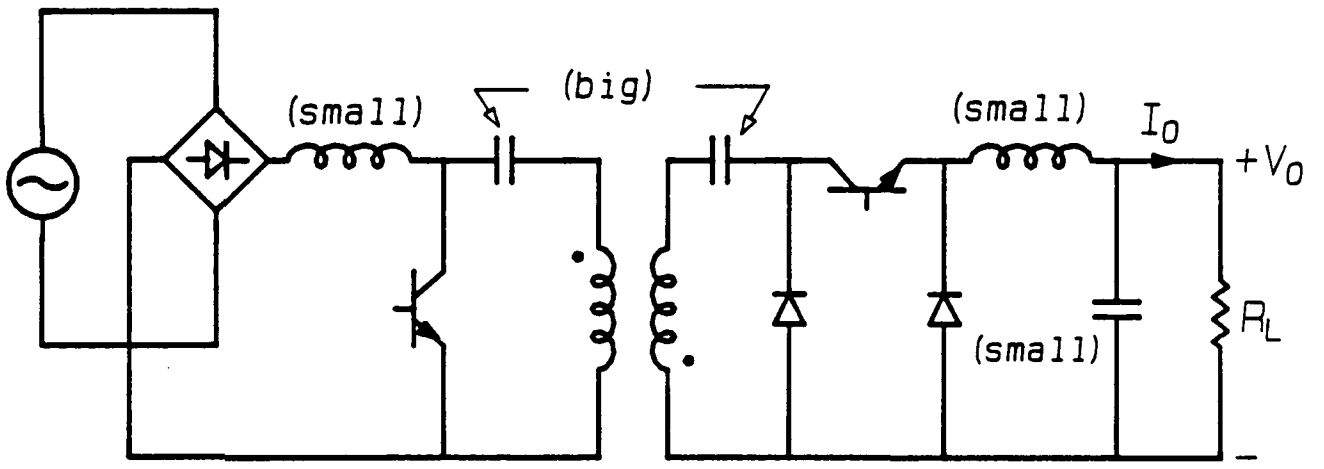

Figure 28: Isolated 3SN Ćuk topology.

6 Conclusions

There are many ways to shape the input current drawn by a single-phase ac-to-dc power converter. The preceding sections have discussed passive and active input-current shaping methods, alternative ways to meet stored energy requirements, and a topology modification that allows rapid output voltage regulation. The methods presented are some of the most promising, but many other variations certainly exist. The designer's task is to decide how much current shaping is necessary or practical and which of the various schemes should be used. To aid in this decision, the relative merits and drawbacks of the current-shaping methods are now discussed, with emphasis on certain applications.

Perhaps the most important feature of a current-shaping application is the amount of power to be processed. At high power levels, the designer has few options. Capacitors are nearly out of the question because of large rms currents. Switch stresses must be kept as low as possible, and switching frequencies will not be much higher than the line frequency. For several reasons, at very high power levels a slow-switching buck topology, such as the sawtooth modulation scheme of Section 3.2.2, will be the preferred choice of all the alternatives presented here.

First, assuming fast voltage regulation will be sacrificed, an active current-shaping scheme with built-in voltage regulation is easier to implement at high power than a large passive filter followed by a complete dc-to-dc converter. Second, a buck topology can easily achieve $\cos\phi = 1$, no matter how slowly it is switched, simply by using symmetrical modulation, as illustrated in Fig.29. A boost topology needs a complicated control scheme to have an in-phase fundamental component of current, and the control must change with the load. The PF for a buck topology, however, is independent of the load, because as the load changes only the *amplitude* of the current pulses in Fig.29 need change, not the switching times. In addition, the buck feeds a nearly constant current into the parallel combination of output capacitor and load, while the boost has a discontinuous current waveform. The buck consequently has a higher quality output voltage, with less ripple and noise. Finally, boost topologies have a capacitor with large rms current. If the input current of a buck topology is not filtered, the topology does not need a high current capacitor. The buck topology therefore allows one to avoid capacitors with large rms currents, but only at the expense of the poor current waveform of Fig.29, with its large harmonic content and high di/dt. (*Any* current-shaping method, active or passive, with smooth, high quality line current will have at least one capacitor with rms current on the order of the line current.)

"Current shaping" becomes a fuzzy concept at high power levels. Low harmonic content and good PF are still goals, but the demands of high power usually force the designer to settle for small fundamental phase displacement ($\cos\phi \approx 1$) and whatever harmonic content comes with it. (In fact, the phrase "unity PF" at high power levels is often misleading, frequently referring only to $\cos\phi = 1$, not true unity PF.) The input current of Fig.29 does not seem to deserve the description "shaped," but at high power levels such waveforms are common and are considered "good."

When power levels are low enough to permit fast-switching, more options are available. Before choosing one, the designer must decide just how good the current waveshape should be. Unity PF is certainly desirable, but most specifications do not call for perfect sine wave input currents. Power level and cost constraints can, and often do,

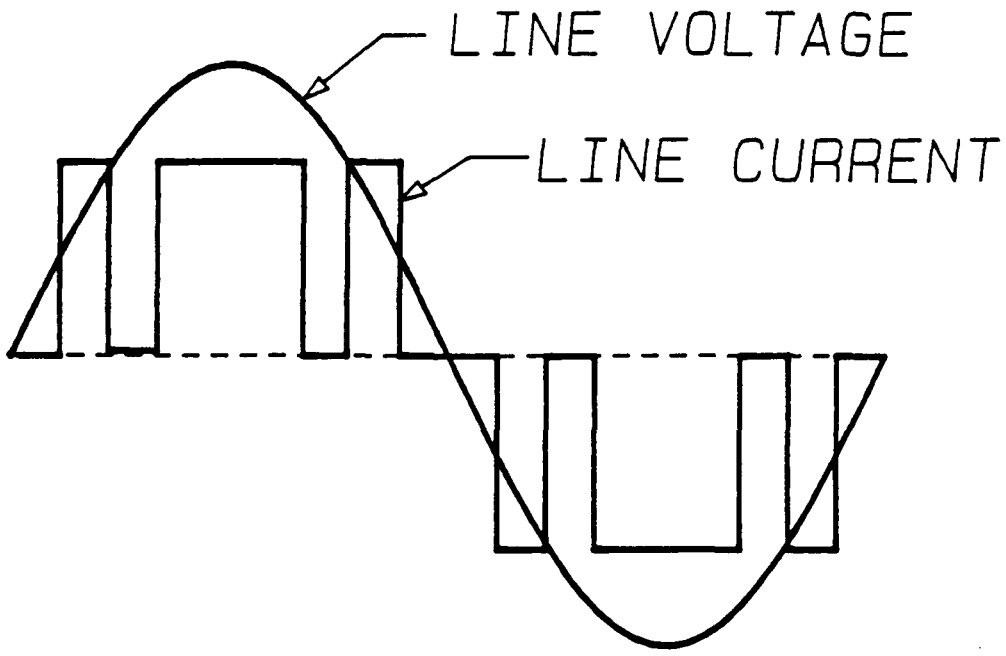

Figure 29: Line current of a buck topology when switching frequency is very low.

force one to accept less than ideal PF's and current waveforms. For applications where near-unity PF is practical and fast-switching schemes are being considered, the following specific recommendations can be made:

- When switching frequency is fairly high in an active resistor emulation scheme (buck or boost), a resonant filter should be used to allow lower weight and faster control, unless the extra stored energy of a large capacitor or inductor is needed anyway to meet hold-up time specifications.

- When power levels permit fast switching, a boost-based topology is preferred to a buck-derived topology. The input current is cleaner and requires no filter.

- If active current shaping is employed and fast output voltage regulation is desired, the 3SN topologies appear to provide a simpler power processor than a cascade of current shaper and dc-to-dc converter. Application of these topologies to current shaping needs further investigation.

- In a noisy environment, the boost converter operating in DCM has the advantage of requiring no high-bandwidth control loop (such as current programming) to shape the input current.

- In the unusual case of a high line frequency, passive methods should be given extra attention. The reactive elements will be smaller, and once the passive circuit generates a dc voltage, the dc-to-dc post-regulator can switch at any frequency—even below the line frequency.

- For applications where the load will change over a broad range, active methods—and buck-based topologies in particular—are better able to impose a constant PF and current waveshape than passive methods.

On the system level, a question that needs further investigation concerns central versus distributed current shaping. Is it better to have a high power current-shaped ac-to-dc converter that generates a dc bus voltage which supplies individual dc-to-dc converters? Or would there be more advantages to a distributed scheme in which the single-phase ac line voltage is bussed, and each local power processor performs its own current shaping?

It is unfortunate that input-current shaping is a luxury one can only afford at low to medium power levels; most of the noise and power factor damage to the utility lines is caused by high power systems. As pollution of the power lines becomes a more pressing problem, however, emphasis will shift toward better input-side performance, and the fast-switching methods emphasized in this report will become more attractive. The methods presented here offer a wide variety of means to shape current and perform the tasks that go along with it, such as energy storage and voltage regulation. The designer should be aware of the many techniques available and choose the method most appropriate to the particular application.

Appendices

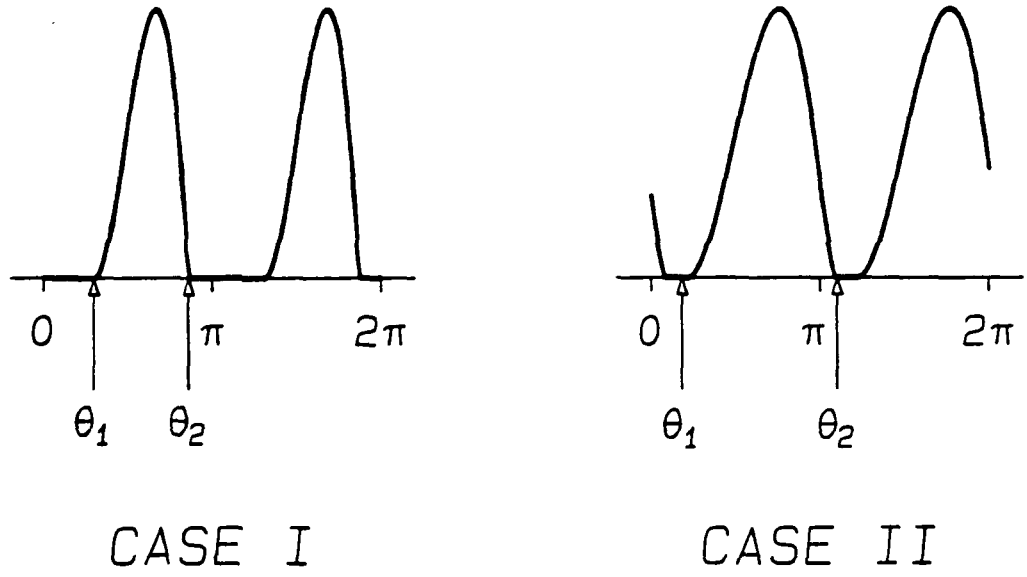

Figure 30: Inductor current waveforms for discontinuous mode of operation of the inductor input filter.

A Discontinuous Conduction Mode of the Inductor Input Filter

This section studies the discontinuous mode of operation of the inductor input filter of Fig.3. For convenience, define

$$\theta \equiv \omega t \tag{44}$$

The analysis is divided into two cases, corresponding to the two inductor current waveforms of Fig.30. In both cases, conduction of the bridge rectifiers begins when the input voltage rises to meet the output voltage. The angle θ_1 is defined as the value of θ at this instant, giving the relation

$$\frac{V}{V_g} = \sin\theta_1 \tag{45}$$

The angle θ_2 is defined as the value of θ at the instant the inductor current reaches zero. For case I of Fig.30, θ_2 lies in the same half-cycle of the line voltage as θ_1, or $\theta_2 < \pi$. Case II occurs when the inductor current extends into the next half-cycle, and $\theta_2 > \pi$.

The input current for case I is found from

$$i_g(\theta) = \frac{1}{\omega L}\int_{\theta_1}^{\theta}(V_g \sin\theta' - V)\, d\theta' \quad , \quad \theta_1 < \theta < \pi \tag{46}$$

Using Eq.(45) for V and evaluating the integral gives

$$i_g = \frac{V_g}{\omega L}\left[\cos\theta_1 - \cos\theta - (\theta - \theta_1)\sin\theta_1\right] \tag{47}$$

The cut-off angle θ_2 is found by solving

$$\cos\theta_1 - \cos\theta_2 - (\theta_2 - \theta_1)\sin\theta_1 = 0 \tag{48}$$

This transcendental equation must be solved before K_l or the PF can be found. Once θ_2 is known, however, K_l can be calculated by integrating $i_g(\theta)$ from θ_1 to θ_2 to find the average inductor current. Since

$$R = \frac{V}{i_{avg}} = \frac{V_g \sin\theta_1}{i_{avg}} \tag{49}$$

K_l can be written in terms of θ_1 and θ_2.

$$K_l = \frac{1}{\pi^2 \sin\theta_1}\left\{\sin\theta_1[1 - \frac{1}{2}(\theta_2 - \theta_1)^2] - \sin\theta_2 + (\theta_2 - \theta_1)\cos\theta_1\right\} \tag{50}$$

The angle θ_2 is a function only of θ_1. The function Eq.(50) is one-to-one, so that θ_1 can be considered a function of K_l. (This means that given K_l, θ_1 is uniquely determined. No two different values of θ_1 result from the same K_l.)

To find the power factor, Eq.(46) is first squared and integrated over the range $\theta_1 < \theta < \theta_2$, yielding

$$\begin{aligned} i^2_{g\,\mathrm{rms}} = \left(\tfrac{V_g}{\omega L}\right)^2 \tfrac{1}{\pi}\Big\{\tfrac{1}{3\sin\theta_1}\Big(&[(\theta_2 - \theta_1)\sin\theta_1 - \cos\theta_1]^3 + \cos^3\theta_1\Big) \\ &+ \tfrac{1}{2}(\theta_2 - \theta_1) + \tfrac{1}{4}\sin 2\theta_2 + 2(\theta_2 - \theta_1)\sin\theta_1\sin\theta_2 \\ &- \tfrac{1}{2}\sin\theta_1\cos\theta_2 - 2\sin(\theta_2 - \theta_1)\Big\} \end{aligned} \tag{51}$$

The PF is then evaluated using

$$\mathrm{PF} = \frac{\sqrt{2} i_{g\,\mathrm{avg}} \sin\theta_1}{i_{g\,\mathrm{rms}}} \tag{52}$$

where $i_{g\,\mathrm{avg}}$ is given by

$$i_{g\,\mathrm{avg}} = \frac{V_g}{\omega L}\pi K_l \sin\theta_1 \tag{53}$$

The fundamental phase displacement component of the PF, $\cos\phi$, is found by evaluating the Fourier coefficients of the fundamental of Eq.(46). The cosine coefficient is

$$\begin{aligned} a_1 = \tfrac{2}{\pi}\Big[&\sin(\theta_2 - \theta_1) - (\theta_2 - \theta_1)(\tfrac{1}{2} + \sin\theta_1\sin\theta_2) \\ &- \tfrac{1}{4}(\sin 2\theta_2 - \sin 2\theta_1)\Big] \end{aligned} \tag{54}$$

and the sine coefficient is

$$\begin{aligned} b_1 = \tfrac{2}{\pi}\Big[&(\theta_2 - \theta_1)\sin\theta_1\cos\theta_2 - \cos(\theta_2 - \theta_1) \\ &+ 1 + \tfrac{1}{2}(\cos^2\theta_2 - \cos^2\theta_1)\Big] \end{aligned} \tag{55}$$

The phase displacement factor is then given by

$$\cos\phi = \frac{b_1}{\sqrt{a_1^2 + b_1^2}} \tag{56}$$

The boundary between cases I and II occurs when $\theta_2 = \pi$. The value of θ_1 corresponding to this from Eq.(48) is approximately .8105 radians, about 46 degrees. The conduction parameter K_l is approximately .362 at this boundary. The boundary between cases I and II also marks the change between continuous and discontinuous line current. For $K_l > .362$, the line current is discontinuous.

For case II of Fig.30, analysis proceeds just as in case I except that for $\theta > \pi$ the voltage from the bridge is $-\sin\theta$, to account for the rectification of the sine wave voltage. The inductor current now follows Eq.(46) for $\theta_1 < \theta < \pi$, but for $\pi < \theta < \theta_2$,

$$i_g(\theta) = \frac{V_g}{\omega L}\left[(2 + \cos\theta_1 + \theta_1 \sin\theta_1) + \cos\theta - \theta\sin\theta_1\right] \tag{57}$$

The cut-off angle θ_2 is found by solving

$$2 + \cos\theta_1 + \theta_1\sin\theta_1 + \cos\theta_2 - \theta_2\sin\theta_1 = 0 \tag{58}$$

For case II, the conduction parameter K_l is

$$\begin{aligned} K_l = \tfrac{1}{\pi^2 \sin\theta_1}\Big\{&\sin\theta_1\left[1 - \tfrac{1}{2}(\theta_2 - \theta_1)^2\right] \\ &+2(\theta_2 - \pi) + (\theta_2 - \theta_1)\cos\theta_1 + \sin\theta_2\Big\} \end{aligned} \tag{59}$$

The expression for the rms inductor current is even more unwieldy:

$$\begin{aligned} i_{g\,\mathrm{rms}}^2 = \left(\tfrac{V_g}{\omega L}\right)^2 \tfrac{1}{\pi}\Big\{&\tfrac{1}{3\sin\theta_1}\left([(\theta_2 - \theta_1)\sin\theta_1 - \cos\theta_1]^3 + \cos^3\theta_1\right) \\ &+ (\theta_2 - \theta_1)(\tfrac{1}{2} - 2\sin\theta_1\sin\theta_2) + 2\sin(\theta_2 - \theta_1) \\ &+ 4(\sin\theta_2 - \sin\theta_1) + \tfrac{1}{4}(\sin 2\theta_1 - \sin\theta_1) \\ &+4(\theta_2 - \pi)(1 + \cos\theta_1 + \theta_1\sin\theta_1 - \tfrac{1}{2}(\theta_2 + \pi)\sin\theta_1)\Big\} \end{aligned} \tag{60}$$

The PF for case II is evaluated as for case I, using the new expressions Eqs.(60) and (59) for $i_{g\,\mathrm{rms}}$ and K_l, respectively. Equation (53) still gives the average current in terms of the appropriate K_l for that mode.

The Fourier coefficients for the current fundamental in case II are

$$\begin{aligned} a_1 = \tfrac{2}{\pi}\Big\{&-\sin(\theta_2 - \theta_1) - \tfrac{1}{4}(\sin 2\theta_2 - \sin 2\theta_1) + \tfrac{1}{2}(\theta_1 - \theta_2) \\ &+ (\theta_2 - \theta_1)\sin\theta_1\sin\theta_2 - 2\sin\theta_2 + 2\sin\theta_1\Big\} \end{aligned} \tag{61}$$

and

$$\begin{aligned} b_1 = \tfrac{2}{\pi}\{&-(\theta_2 - \theta_1)\sin\theta_1\cos\theta_2 + 2\cos\theta_1 + 2\cos\theta_2 \\ &+ \cos(\theta_2 - \theta_1) + \tfrac{1}{4}(\cos 2\theta_2 - \cos 2\theta_1) + 3 - 2(\pi - \theta_1)\sin\theta_1\Big\} \end{aligned} \tag{62}$$

The phase displacement factor is again given by

$$\cos\phi = \frac{b_1}{\sqrt{a_1^2 + b_1^2}} \tag{63}$$

B Analysis of the Resonant Input Filter

This section outlines the analysis of the resonant input filter of Fig.7. The following assumptions are used:

- Input voltage is a perfect sine wave, $V_g \sin\omega t$.
- The capacitor C_∞ is large enough that the output voltage may be considered a pure dc voltage V.
- The unloaded Q of the series resonant circuit $L-C$ is infinite—there is no parasitic series resistance.
- The diode bridge is considered ideal.

It is also assumed that the resonant frequency of the filter,

$$\omega_0 = \frac{1}{\sqrt{LC}}$$

is equal to the line frequency ω, since this results in optimum performance. Define $\theta \equiv \omega t$ and

$$Z_0 \equiv \sqrt{\frac{L}{C}}$$

Since the resonant frequency and line frequency are the same, Z_0 is equal to ωL.

Continuous Conduction Mode

Consider the resonant current waveform of Fig.31. It is not immediately apparent that the diode bridge will switch at $\theta = 0$ and $\theta = \pi$. Instead, assume that the bridge switches at time θ_1 when the current i_L passes through zero. From θ_1 to $\pi + \theta_1$ the resonant current satisfies the differential equation

$$\frac{d^2}{d\theta^2} i_L + i_L = \frac{V_g}{Z_0} \cos\theta \tag{64}$$

Natural solutions to this equation are $\cos\omega t$ and $\sin\omega t$ and the particular solution is

$$\frac{V_g}{2Z_0} \theta \sin\theta \tag{65}$$

The total current during the period $\theta_1 < \theta < \pi + \theta_1$ is then

$$i_L(\theta) = A\cos\theta + B\sin\theta + \frac{V_g}{2Z_0}\theta\sin\theta \tag{66}$$

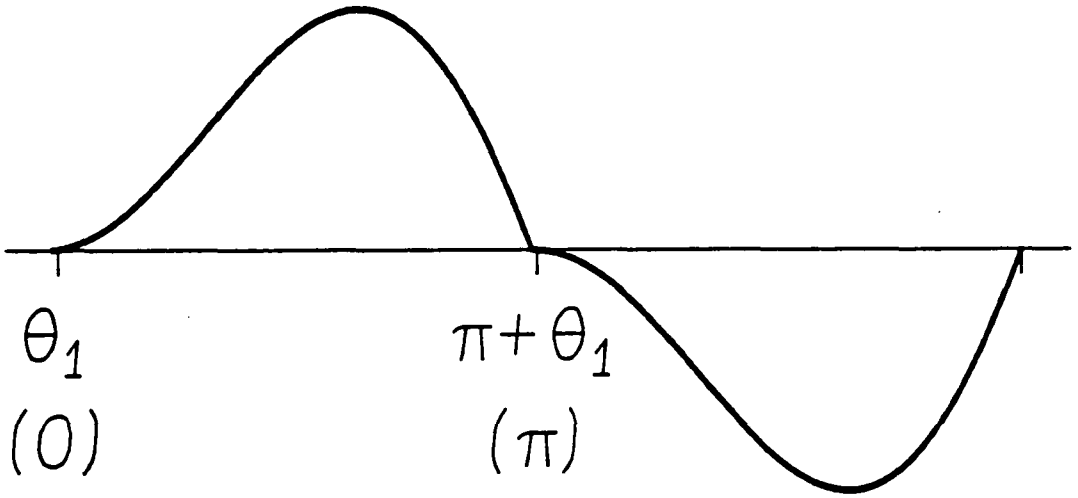

Figure 31: Inductor current waveform for the resonant input filter in continuous conduction mode.

Four unknown quanties must be determined: θ_1, A, B, and the magnitude of the output voltage V, which does not appear in the equation for i_L.

Applying the condition that the current is zero at both θ_1 and at $\pi + \theta_1$ gives $\theta_1 = 0$ and $\theta_1 = \pi$ as the only admissible values of θ_1, and only $\theta_1 = 0$ gives positive power flow through the filter. Then, using $i_L(0) = 0$ implies that $A = 0$.

Since $\theta_1 = 0$, the switching of the bridge applies a square wave voltage of magnitude V to one side of the series resonant circuit. By assumption, the circuit has no parasitic resistance. Stable operation therefore requires zero net voltage across the resonant circuit at the resonant frequency. This is only possible when the fundamental component of the rectifier-switched output voltage is equal in magnitude to the input voltage, or

$$\frac{4}{\pi}V = V_g, \quad \text{or} \quad \frac{V}{V_g} = \frac{\pi}{4} \tag{67}$$

Finally, the constant B is determined by equating the average input current during a half-cycle with the average output current:

$$\frac{1}{\pi}\int_0^{\pi} i_L(\theta)\, d\theta = I = \frac{V}{R} \tag{68}$$

This leads to

$$B = \frac{\pi}{4}\frac{V_g}{Z_0}\left(\frac{\pi^2}{2}K_l - 1\right) \tag{69}$$

where

$$K_l \equiv \frac{\omega L}{\pi R} \tag{70}$$

This is the same conduction parameter defined for the inductor input filter. The final expression for the current over the half-cycle $0 < \theta < \pi$ is then

$$i_L = \frac{V_g}{2Z_0}\left[\theta \sin\theta + \frac{\pi}{4}\left(\frac{\pi^2}{4}K_l - 1\right)\sin\theta\right] \tag{71}$$

With the current waveform known, the average (over a half-cycle) and rms line currents can be calculated. The average output current I equals the average of the line current over the interval $0 < \theta < \pi$.

$$I = i_{L\,\mathrm{avg}} = \frac{V_g}{2Z_0}\frac{\pi^2}{2}K_l \tag{72}$$

The rms line current is found by averaging the square of Eq.(71) over a half-cycle.

$$i_{L\,\mathrm{rms}} = \left(\frac{V_g}{2Z_0}\right)\frac{\pi^3}{4\sqrt{2}}\sqrt{K_l^2 + \frac{4}{3\pi^4} - \frac{8}{\pi^6}} \tag{73}$$

Finally, the power factor is calculated as the ratio of output power, VI, to the product of rms line voltage and current.

$$\mathrm{PF} = \frac{K_l}{\sqrt{K_l^2 + \frac{4}{3\pi^4} - \frac{8}{\pi^6}}} \approx \frac{1}{\sqrt{1 + \left(\frac{0.073}{K_l}\right)^2}} \tag{74}$$

In continuous conduction mode the current i_L must be positive throughout the interval $0 < \theta < \pi$. Since $i_L(0) = 0$, the initial slope of the current must also be positive, and this means B must be positive. From Eq.(69), therefore, the boundary between CCM and DCM is

$$K_{l\,\mathrm{crit}} = \frac{2}{\pi^2} \tag{75}$$

Discontinuous Conduction Mode

Figure 32 shows a half-cycle of resonant current in DCM. The current in DCM still obeys Eq.(66), but the values A and B must be found, and θ_1 will be different from zero. Two conditions are applied to find A and B: first, $i_L(\theta_1) = 0$, and second, the slope of i_L must also be zero at θ_1. In DCM, the diode bridge is cut-off until the input voltage minus the capacitor voltage just equals the output voltage. This occurs at θ_1 and there is no voltage on the inductor at this instant, hence $di_L/d\theta = 0$ at $\theta = \theta_1$. These two conditions give simultaneous equations in A and B, with the solutions

$$\begin{aligned} A &= \tfrac{V_g}{2Z_0}\sin^2\theta_1 \\ B &= -\tfrac{V_g}{2Z_0}\left(\theta_1 + \sin\theta_1\cos\theta_1\right) \end{aligned} \tag{76}$$

The final expression for i_L in DCM is

$$i_L = \frac{V_g}{2Z_0}\left[(\theta - \theta_1)\sin\theta - \sin\theta_1\sin(\theta - \theta_1)\right] \tag{77}$$

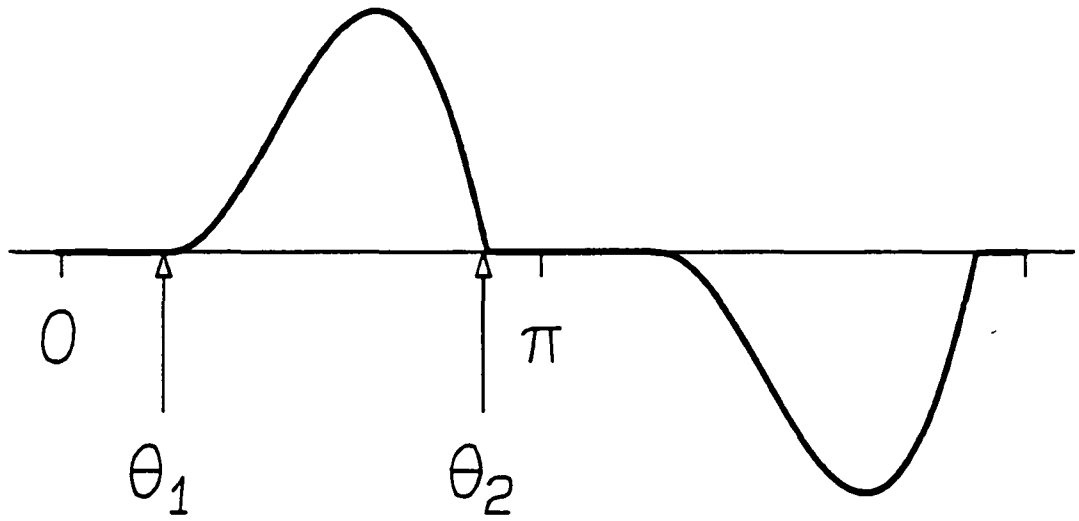

Figure 32: Inductor current waveform of the resonant input filter in discontinuous conduction mode.

Setting $i_L(\theta_2) = 0$ leads to the following implicit expression for θ_2:

$$(\theta_2 - \theta_1)\sin\theta_2 - \sin\theta_1 \sin(\theta_2 - \theta_1) = 0 \tag{78}$$

Finding the output voltage is somewhat laborious. First the voltage waveform is found to within a constant by using

$$v_C = \frac{1}{\omega C}\int i_L(\theta)\, d\theta \tag{79}$$

Then, cyclic stability requires that

$$v_C(\theta_2) = -v_C(\theta_1) \tag{80}$$

and this yields the constant, giving

$$\begin{aligned} v_C(\theta) = \tfrac{V_g}{4}\Big[&\sin\theta_1\,(2\cos(\theta - \theta_1) - \cos(\theta_2 - \theta_1) - 2) \\ &-2(\theta - \theta_1)\cos\theta + 2\sin\theta + (\theta_2 - \theta_1)\cos\theta_2 - \sin\theta_2\Big] \end{aligned} \tag{81}$$

Finally, the output voltage is determined from the fact that, when the bridge first turns on,

$$V_g \sin\theta_1 - v_C(\theta_1) = V \tag{82}$$

which leads to

$$\frac{V}{V_g} = \frac{1}{4}\left\{\Big[2 + \cos(\theta_2 - \theta_1)\Big]\sin\theta_1 + \sin\theta_2 - (\theta_2 - \theta_1)\cos\theta_2\right\} \tag{83}$$

The average output current, found by integrating $i_L(\theta)$ over a half-cycle, is

$$I = \left(\frac{V_g}{2Z_0}\right)\frac{1}{\pi}\left\{\sin\theta_1\left[\cos(\theta_2-\theta_1)-2\right]+\sin\theta_2-(\theta_2-\theta_1)\cos\theta_2\right\} \tag{84}$$

The mean square line current is calculated by averaging $i_L^2(\theta)$, yielding the following complicated expression.

$$i_{L\,\mathrm{rms}}^2 = \left(\frac{V_g}{2Z_0}\right)^2\frac{1}{4\pi}f(\theta_1,\theta_2) \tag{85}$$

where

$$\begin{aligned} f(\theta_1,\theta_2) = &\left\{\tfrac{2}{3}(\theta_2-\theta_1)^3-(\theta_2-\theta_1)^2\left[\sin 2\theta_1+\sin 2\theta_2\right]\right. \\ &+(\theta_2-\theta_1)\left[1+\cos 2(\theta_2-\theta_1)-\cos 2\theta_1-2\cos 2\theta_2\right] \\ &\left.-(\theta_2-\theta_1)^2\sin 2\theta_2-\sin 2\theta_1-\left[1-\tfrac{1}{2}\cos 2\theta_1\right]\sin 2(\theta_2-\theta_1)\right\} \end{aligned} \tag{86}$$

Applying the previous results to the definition of PF gives the following expression:

$$\mathrm{PF} = \frac{g(\theta_1,\theta_2)}{\sqrt{2\pi f(\theta_1,\theta_2)}} \tag{87}$$

where

$$\begin{aligned} g(\theta_1,\theta_2) = &\left\{\left[2+\cos(\theta_2-\theta_1)\right]\sin\theta_1+\sin\theta_2-(\theta_2-\theta_1)\cos\theta_2\right\} \\ &\times\left\{\sin\theta_1\left[\cos(\theta_2-\theta_1)-2\right]+\sin\theta_2-(\theta_2-\theta_1)\cos\theta_2\right\} \end{aligned} \tag{88}$$

The expression for I can also be used to find R in terms of θ_1 and θ_2, which then leads to K_l:

$$K_l = \frac{2}{\pi^2}\left[\frac{\sin\theta_1\left[\cos(\theta_2-\theta_1)-2\right]+\sin\theta_2-(\theta_2-\theta_1)\cos\theta_2}{\sin\theta_1\left[\cos(\theta_2-\theta_1)+2\right]+\sin\theta_2-(\theta_2-\theta_1)\cos\theta_2}\right] \tag{89}$$

As in the inductor input filter, K_l is a one-to-one function of θ_1, so that one may instead consider θ_1 to be a function of K_l. Both θ_1 and θ_2 are determined by K_l alone, and the PF is therefore a function of K_l alone. To plot the PF in DCM, a value of θ_1 is chosen and θ_2 calculated by numerically solving Eq.(78). Then K_l and the PF can be calculated and plotted versus each other.

Bibliography

[1] F.C. Schwarz, "A Time-Domain Analysis of the Power Factor for Rectifer System with Over- and Subcritical Inductance," IEEE Trans. on Industrial Electronics and Control Instrumentation, Vol. IECI–20, No.2, May 1973, pp.61–68.

[2] S.B. Dewan, "Optimum Input and Output Filters for a Single-Phase Rectifier Power Supply," IEEE Trans. on Industry Applications, Vol. IA–17, No.3, May/June 1981, pp.282–288.

[3] R. Keller and G. Baker, "Unity Power Factor Off-Line Switching Power Supplies," Proc. Intelec '84, pp.332–339 (IEEE Publication 84CH2073–5).

[4] W.E. Rippel, "Optimizing Boost Chopper Charger Design," Proc. PowerCon 6, May 1979, pp.D1–1 to D1–20.

[5] D. Chambers and D. Wang, "Dynamic P.F. Correction in Capacitor Input Off-Line Converters," Proc. PowerCon 6, May 1979, pp.B3–1 to B3–6.

[6] N.J. Barabas, "Simplified Control Algorithm for Active Power Factor Correction," Proc. PCI '85 (October 1985), pp.1–9.

[7] R. Mahadevan, S. El-Hamamsy, W.M. Polivka and S. Ćuk, "A Converter with Three Switched-Networks Improves Regulation, Dynamics, and Control," Proc. PowerCon 10, March 1983, pp.

[8] T. Wolpert, "Active Filter Technique for the Attenuation of Ac Ripple in Dc Power Plants and Distribution," Proc. Intelec '84, pp.461–467 (IEEE Publication 84CH2073–5).

[9] M.J. Kocher and R.L. Steigerwald, "An Ac to Dc Converter with High Quality Input Waveforms," IEEE Power Electronics Specialists Conference, 1982 Record, pp.63–75 (IEEE Publication 82CH1762–4)

[10] T. Kataoka, K. Mizumachi and S. Miyairi, "A Pulse-Width Controlled Ac to Dc Converter to Improve Power Factor and Waveform of Ac Line Current," Proc. IEEE International Semiconductor Power Converter Conference, Orlando Fl., March 1977, pp. 334–339.

[11] M.F. Schlecht, "Novel Topological Alternatives to the Design of a Harmonic-Free Utility/Dc Interface," IEEE Power Electronics Specialists Conference, 1983 Record, pp.206–216 (IEEE Publication 83CH1877–0).

[12] I.A. Khan and R.W. Erickson, "Control of Switched-Mode Converter Harmonic-Free Terminal Waveforms through Internal Energy Storage," paper to be presented at the 1986 Power Electronics Specialists Conference.